NAVAL POSTGRADUATE SCHOOL

MONTEREY, CALIFORNIA

THESIS

PERFORMANCE CHARACTERIZATION OF A MOBILE MICROGRID

by

Robert C. Lindstrom

September 2022

Thesis Advisor: Giovanna Oriti
Co-Advisors: Preetha Thulasiraman
Douglas L. Van Bossuyt

THIS PAGE INTENTIONALLY LEFT BLANK

REPORT DOCUMENTATION PAGE			*Form Approved OMB No. 0704-0188*

1. AGENCY USE ONLY *(Leave blank)*	**2. REPORT DATE** September 2022	**3. REPORT TYPE AND DATES COVERED** Master's thesis

4. TITLE AND SUBTITLE
PERFORMANCE CHARACTERIZATION OF A MOBILE MICROGRID

5. FUNDING NUMBERS

6. AUTHOR(S) Robert C. Lindstrom

7. PERFORMING ORGANIZATION NAME(S) AND ADDRESS(ES)
Naval Postgraduate School
Monterey, CA 93943-5000

8. PERFORMING ORGANIZATION REPORT NUMBER

9. SPONSORING / MONITORING AGENCY NAME(S) AND ADDRESS(ES)
N/A

10. SPONSORING / MONITORING AGENCY REPORT NUMBER

11. SUPPLEMENTARY NOTES The views expressed in this thesis are those of the author and do not reflect the official policy or position of the Department of Defense or the U.S. Government.

12a. DISTRIBUTION / AVAILABILITY STATEMENT
Approved for public release. Distribution is unlimited.

12b. DISTRIBUTION CODE
A

13. ABSTRACT (maximum 200 words)

With a rising global emphasis on the use of renewable energy and the reduction of fossil fuels, the Department of Defense is incorporating microgrid technology into energy management systems at forward-deployed and domestic installations. Understanding the nature of the connection between a microgrid and the local utility grid is critical in determining if sensitive loads will be adequately supported. IEEE Standard 1547–2018 applies to this interconnection and specifies the technical requirements and limitations for normal and abnormal operation and expectations for interrupting events. A commercial-off-the-shelf (COTS) microgrid is tested for its compliance to this standard and also for characteristics, such as efficiency, that help define its operational capability. The microgrid can operate in a grid-connected state or an islanded state, disconnected from the utility grid, if the grid is unavailable or if the power quality is unable to support military operations. A microgrid testbed was set up that included the individual COTS components, a centralized control system and several measurement instruments connected that read voltages and currents continuously throughout the experiments. By observing the microgrid functionality, this thesis created an objective characterization template that can be used to assess the capabilities of other COTS microgrids to determine whether they are capable of supporting sensitive loads on forward-deployed or domestic military installations.

14. SUBJECT TERMS distributed energy resource, DER, commercial off-the-shelf, COTS, microgrid, environmental	**15. NUMBER OF PAGES** 99
	16. PRICE CODE

17. SECURITY CLASSIFICATION OF REPORT	**18. SECURITY CLASSIFICATION OF THIS PAGE**	**19. SECURITY CLASSIFICATION OF ABSTRACT**	**20. LIMITATION OF ABSTRACT**
Unclassified	Unclassified	Unclassified	UU

NSN 7540-01-280-5500

Standard Form 298 (Rev. 2-89)
Prescribed by ANSI Std. 239-18

THIS PAGE INTENTIONALLY LEFT BLANK

Approved for public release. Distribution is unlimited.

PERFORMANCE CHARACTERIZATION OF A MOBILE MICROGRID

Robert C. Lindstrom
Captain, United States Marine Corps
BS, Tennessee Technological University, 2016

Submitted in partial fulfillment of the
requirements for the degree of

MASTER OF SCIENCE IN ELECTRICAL ENGINEERING

from the

NAVAL POSTGRADUATE SCHOOL
September 2022

Approved by: Giovanna Oriti
Advisor

Preetha Thulasiraman
Co-Advisor

Douglas L. Van Bossuyt
Co-Advisor

Douglas J. Fouts
Chair, Department of Electrical and Computer Engineering

THIS PAGE INTENTIONALLY LEFT BLANK

ABSTRACT

With a rising global emphasis on the use of renewable energy and the reduction of fossil fuels, the Department of Defense is incorporating microgrid technology into energy management systems at forward-deployed and domestic installations. Understanding the nature of the connection between a microgrid and the local utility grid is critical in determining if sensitive loads will be adequately supported. IEEE Standard 1547–2018 applies to this interconnection and specifies the technical requirements and limitations for normal and abnormal operation and expectations for interrupting events. A commercial-off-the-shelf (COTS) microgrid is tested for its compliance to this standard and also for characteristics, such as efficiency, that help define its operational capability. The microgrid can operate in a grid-connected state or an islanded state, disconnected from the utility grid, if the grid is unavailable or if the power quality is unable to support military operations. A microgrid testbed was set up that included the individual COTS components, a centralized control system and several measurement instruments connected that read voltages and currents continuously throughout the experiments. By observing the microgrid functionality, this thesis created an objective characterization template that can be used to assess the capabilities of other COTS microgrids to determine whether they are capable of supporting sensitive loads on forward-deployed or domestic military installations.

THIS PAGE INTENTIONALLY LEFT BLANK

Table of Contents

List of Figures

THIS PAGE INTENTIONALLY LEFT BLANK

List of Tables

THIS PAGE INTENTIONALLY LEFT BLANK

List of Acronyms and Abbreviations

AC	alternating current
ANSI	American National Standards Institute
COTS	Commercial-Off-The-Shelf
DC	direct current
DER	distributed energy resource
DOD	Department of Defense
EPS	electric power system
ESS	energy storage system
HBX	High Battery Transfer
IEEE	Institute of Electrical and Electronics Engineers
MP	maximum power
MPPT	maximum power point tracking
PCC	point of common coupling
PoC	point of DER connection
PV	photovoltaic
p.u.	per-unit
RMS	root mean square
RPA	reference point of applicability
SOC	state of charge

TRD total rated-current distortion

UPS Uninterrupted Power Supply

U.S. United States

USMC United States Marine Corps

USN United States Navy

Acknowledgments

Acknowledging everyone who helped me along the way to completing this thesis would require more space than is available, but I will highlight a few individuals. I am thankful to have had the wisdom, guidance and patience of my advisor, Dr. Giovanna Oriti, and of my co-advisors, Dr. Preetha Thulasiraman and Dr. Douglas Van Bossuyt. Particularly, Dr. Oriti consistently provided me not only the technical expertise but also the motivation required to continue.

I am also quite thankful for Mr. Jeff Knight, whose technical knowledge and skills are beyond compare and who was able to help me understand the nuances of the electrical machinery that was used throughout this work.

Finally, I have immense gratitude for my family and closest friends who have listened to me and guided me through the challenging times to be able reach this milestone.

Ad Majorem Dei Gloriam

THIS PAGE INTENTIONALLY LEFT BLANK

CHAPTER 1:
Introduction

This chapter begins with an explanation of the motivation for this research and its importance and relevance to the United States (U.S.) military. The objectives of this thesis are then highlighted so as to provide the reader with a clear understanding of what is to be accomplished through this work. Following the objectives is a collection of related work that provides insight as to the state of the research community with this thesis topic. This chapter concludes with the organization of the thesis and brief summaries of the content of each chapter.

1.1 Motivation

Despite the fluctuating price of oil and major efforts to reduce fuel consumption and become more environmentally sustainable, the Department of Defense (DOD), United States Navy (USN) and United States Marine Corps (USMC) must continue to operate using fossil fuels in remote and domestic locations. The modern technologies used by these organizations require more electrical production (often produced via fossil fuels) and energy consumption than technologies used in the past [1]. A goal, therefore, of these organizations has been to reduce fuel consumption while continuing to provide adequate power to sustain military operations in any environment. This has led to the increased deployment of distributed energy resources (DERs) as an alternative source of power at military installations. DERs are sources of electric power, independent from bulk power systems, that include small-scale power generation sources (e.g. photovoltaic (PV) arrays or wind turbines) and energy storage technologies (e.g. batteries or supercapacitors). DERs provide a lower cost and a higher service reliability than the utility power grid [2]. The DOD has implemented changes that have led to a decrease in the amount of fuel used in the fleet, shown in Figure 1.1, while increasing the percentage of renewable energy used, shown in Figure 1.2. The use of renewable DERs as reliable power generation sources and energy storage systems will be increasingly incorporated into the energy planning systems at all installations, as each organization looks to improve its environmental sustainability.

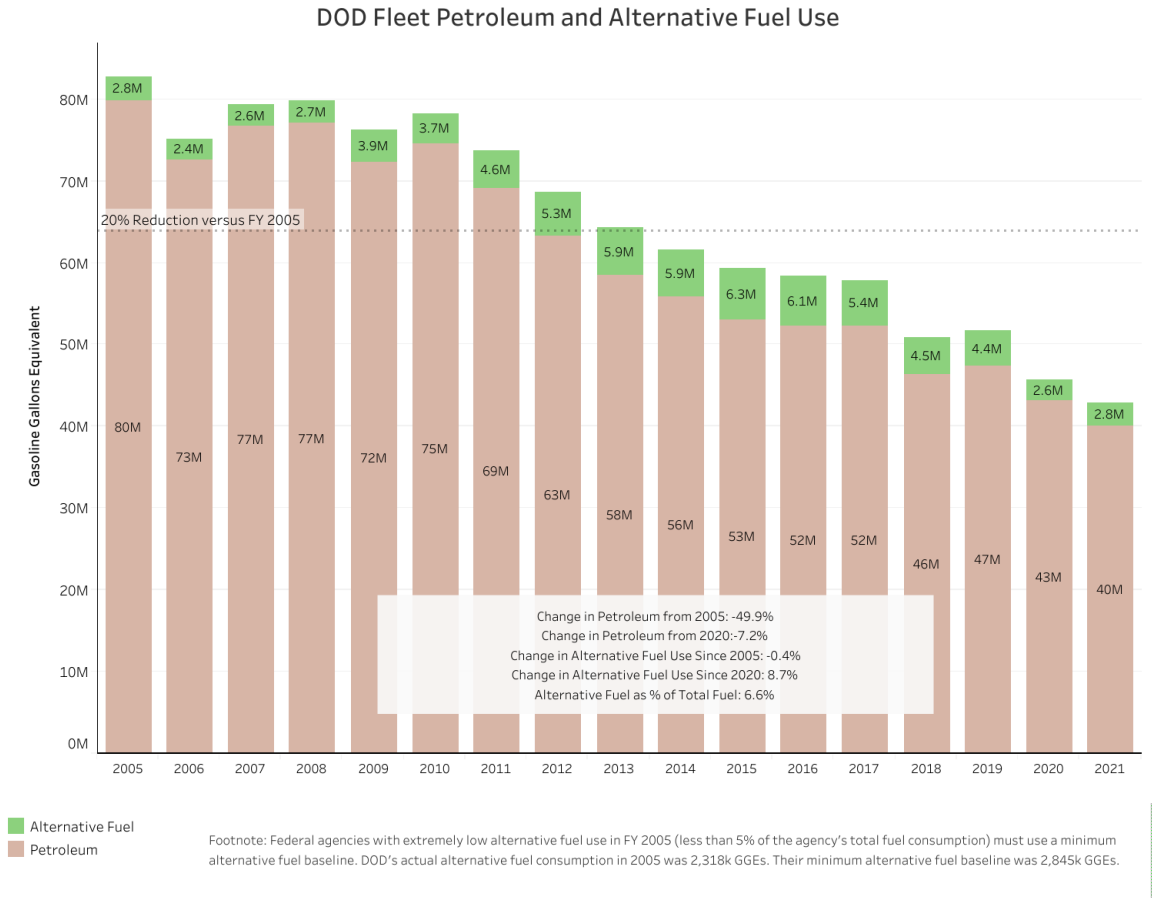

Figure 1.1. DOD fleet fuel use timeline. Source: [3].

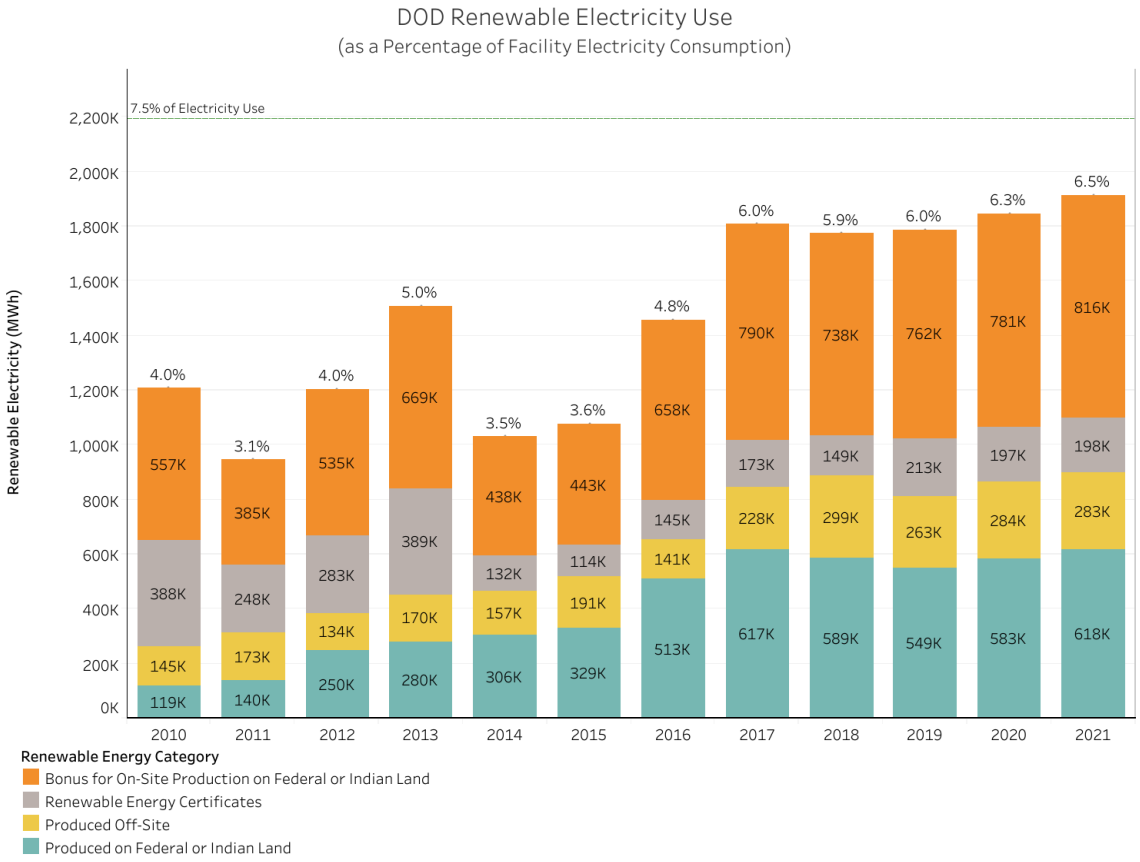

Figure 1.2. DOD renewable electricity use timeline. Source: [3]

The implementation of a microgrid provides energy planners the ability to harness renewable energy from DERs to minimize reliance on the utility grid, thereby decreasing the carbon footprint of the system and enhancing its environmental sustainability. Commercial-Off-The-Shelf (COTS) microgrids are available, but an objective characterization of their performance is not typically provided by the manufacturers. Due to the sensitivity of certain loads found on military installations and the need to provide uninterrupted power to those loads, there must be an understanding of how these COTS products perform in order to determine their potential value for military operations.

The research in this thesis focuses on the adherence of a COTS microgrid to Institute of Electrical and Electronics Engineers (IEEE) Standard 1547-2018 [4]. This standard applies

to the interconnection and interoperability between a DER and the area or local electric power system (EPS) and establishes limitations for normal and abnormal operation and expectations for interrupting events [4]. The adherence of the COTS microgrid to this standard provides an objective characterization that can be used to evaluate its potential for military use.

1.2 Objectives

The objective of this thesis is to analyze the performance characteristics of a COTS microgrid and to compare them against the limits defined by IEEE Standard 1547-2018 in addition to analyzing other characteristics that further define the operational capability of the microgrid. The characteristics tested and analyzed in this research are battery life, voltage and frequency ride-through, transient response to grid failure, steady-state harmonic distortion and balance of system power. The experimental testing and analysis done on these characteristics illustrates the functionality of a COTS microgrid, determines compliance to the standard and provides insight into the realistic use of this microgrid for sensitive loads at military installations. This thesis can be used as a reference tool to characterize COTS microgrids for military operations.

1.3 Related Work

There has been extensive work done since the 2018 revision of IEEE Standard 1547 to assess various functions and requirements at the point of connection between a DER and the utility EPS. Lu identified challenges with large-scale DER penetration of the utility EPS with a series of computer-based simulations in order to propose optimized control methods at the point of interconnection [5]. The work done in [6] explores the simulated fault response of a DER in coordination with the standard and compares that response to a COTS three-phase inverter. The performances of different abnormality or fault detection methods are compared in [7] using a simulated model and a hardware implementation. This research shows that the voltage ride-through requirements of IEEE Standard 1547-2018 are difficult to comply with for highly distorted voltages. Additionally, control strategy performances were compared in [8] to assess voltage abnormalities or faults, and the findings were similar to those of [7]. Ninad created a testbed to assess two COTS three-phase inverter in coordination with

hardware simulators for an EPS and a PV array [9]. This research assessed the voltage, frequency and rate-of-change-of-frequency ride-through capabilities of the inverter and found that the inverters were not in compliance with the standard which was an expected outcome given that they were manufactured prior to the revised requirements. The work done in this thesis complements prior research done on this topic, as it provides an objective outlook of the connection between a DER and the local EPS in a non-simulated environment. Being able to assess whether or not a sensitive load will continue to operate with a COTS microgrid is critical for understanding its relevance to the military community.

1.4 Organization

This thesis is organized to provide the reader with the requisite knowledge needed to visualize and understand the microgrid testbed so that the analysis of the characteristics can be clearly interpreted. Chapter 2 contains background information regarding microgrids in addition to a summary of IEEE Standard 1547-2018 so that the characteristics have clear limitations in order to evaluate compliance. Chapter 3 provides a visualization of the microgrid testbed and detailed explanations of each microgrid component and the measurement instruments used in the experiments. Chapter 4 highlights each of the characteristics that were tested on the microgrid. Each section of Chapter 4 explains why the characteristics are regarded as important and provides the testing methodology, details, results and analysis of each test. This thesis concludes with Chapter 5, which provides conclusions for the work completed and recommendations for future work.

THIS PAGE INTENTIONALLY LEFT BLANK

CHAPTER 2:
Background

In this chapter, general concepts and terms about microgrids are defined and explained. A review of IEEE Standard 1547-2018 is also provided as the standard by which the microgrid in this thesis was compared to for compliance.

2.1 Microgrid Overview

A microgrid is a local energy grid with control capabilities that allow it to disconnect from the larger utility grid and operate autonomously [10]. Microgrids are able to produce energy to power a load bank in either a grid-connected operating state or an islanded operating state. In a grid-connected operating state, the microgrid acts as an extension of the area and local EPS and delivers power to the loads directly from the utility grid. An area EPS is a (usually public) network of generators that provide power, and the transmission and distribution of that power, from a centralized hub to radial locations for consumption [11]. A local EPS is an extension of the area EPS and provides locally-distributed power. In an islanded operating state, the microgrid acts as its own power station, converting power from a direct current (DC) DER (e.g. solar, wind) or consuming power from an alternating current (AC) DER (e.g. a diesel generator). For a microgrid that operates in a remote area, disconnected from any local EPS, the energy produced by the DERs must exceed the load demand in order to provide sustainable power. As this is not always the case, a main component of a microgrid is its connection to the local EPS at the point of DER connection (PoC).

Microgrids are comprised of DERs and other system components, to include an energy storage system (ESS) and renewable or non-renewable energy sources, loads, a control system and a connection to the local EPS. All of these components work together within a defined electrical boundary (a key aspect of the identity of a microgrid) that allow the microgrid to be observed by the local EPS as a single entity [12]. A microgrid utilizes DC power from renewable energy resources to either provide power to the ESS that is then converted to provide appropriate power to the loads, or this power is directed to an inverter system that supplies an AC distribution bus. For a microgrid that supplies power to an ESS,

when the energy level of the ESS drops below a specified threshold, the microgrid is able to continue to supply power to the loads with the local EPS or another DER until such a time that the ESS is able to become the primary power supply once again. In this way, the loads use less energy from the local EPS and are more environmentally friendly.

2.2 Review of IEEE Std 1547-2018

This section will provide a summary of the sections outlined in IEEE Standard 1547 (revised in 2018) [4] for the purpose of understanding the scope of the tested characteristics of the COTS microgrid. There are sections in this standard that either do not apply to the microgrid used in this thesis or are not required for its desired characterization profile. These sections are included in the review of the standard but not discussed in great detail.

2.2.1 Standard Overview

This standard specifies the technical requirements for the interconnection and interoperability between an area or local EPS and a DER [4]. It establishes limits for normal and abnormal operation and expectations for interrupting events. This standard has undergone several revisions since its inception in 2003 but remains general enough to be applicable to a wide range of industrial and institutional technologies. There are a variety of interconnection relationships that this standard is applied to for the area EPS, shown in Figure 2.1. The area EPS connects to a local EPS at the point of common coupling (PCC), while a local EPS connects to a DER at the PoC. This standard applies to the DER connection at the PoC. Referencing the EPS divisions in Figure 2.1, this standard does not apply to Local EPS 1, as a connection only to a load is inherently different than a connection to a DER. Local EPS 2 is the connection relationship focused on in this thesis, and this standard applies to that connection. This standard also applies to local EPSs 3, 4 and 5 at either the PoC or the PCC. For local EPSs 4 and 5, if the DER is not capable of meeting the requirements of this standard, a supplemental DER is required. The microgrid used for this thesis is capable of meeting the requirements of the standard on its own and does not require a supplemental DER system.

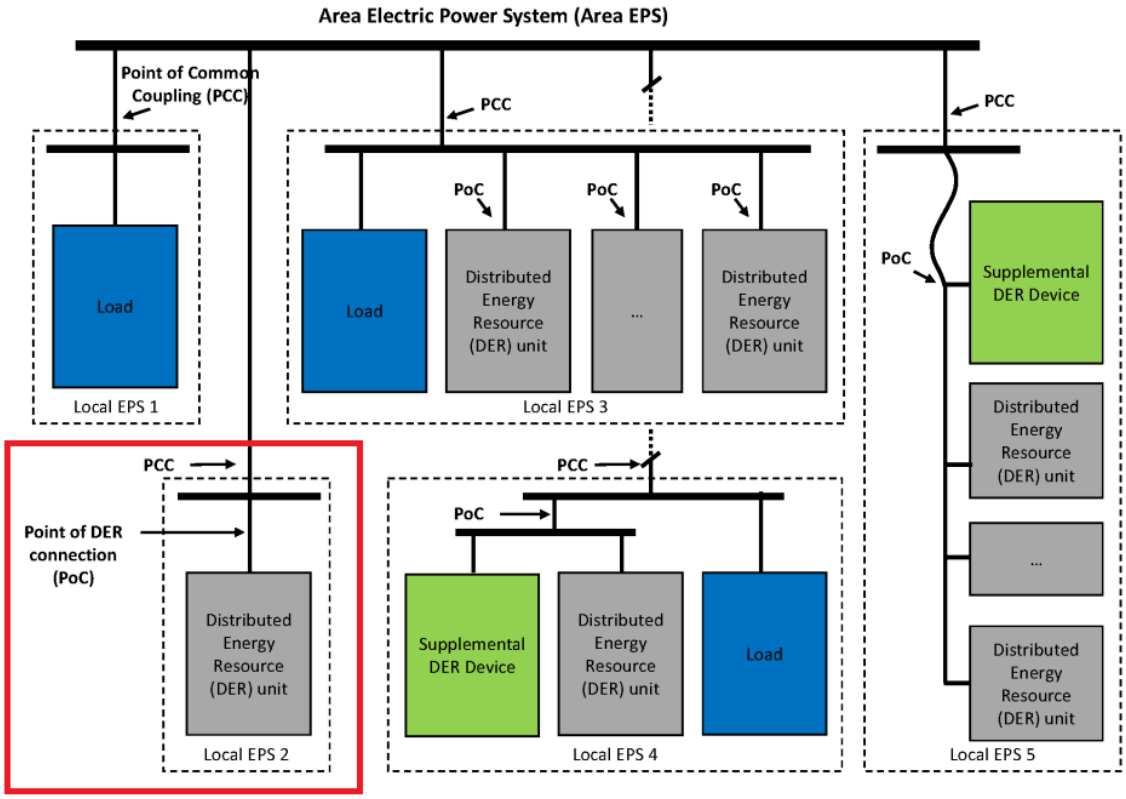

Figure 2.1. The relationship variations for the area EPS are shown here. The red box indicates the type of relationship that is relevant to this thesis. Adapted from [4].

2.2.2 DER Category Assignment

Annex B of the standard provides information regarding the DER category assignment [4]. While out of chronological order for the standard, this section is included before any others as a reference to understand why the information presented in the following sections only applies to a certain category of DER. For the purposes of this thesis, only one category out of three will be included for discussion and analysis.

Taking into account the inherent differences in DER types, regarding voltage and reactive power management and voltage and frequency ride-through capabilities, when interacting

with an area or local EPS, this standard categorizes DERs so as to remain inclusive of various DER technologies. The two sets of categories apply to DERs in this standard: Categories A and B for voltage regulation and reactive power capabilities, and Categories I, II and III for abnormal condition ride-through requirements [4].

The majority of DER systems are categorized as Category B, due to variable-generation power levels. This applies for larger-penetration DER systems, but because of the infrequent nature of the microgrid used in this thesis, only Category B capabilities will be considered.

Assignment to Categories I, II or III is based largely on the security of the bulk power system that is connected to the area or local EPS and the interconnection of the EPS and the DER [4]. To ensure this security is met, a majority of DER systems should be categorized as Category II, and the microgrid used in this thesis, though minimal in DER penetration levels, does not require a Category I assignment.

Therefore, the assignment of the microgrid used in this thesis is Category B for voltage regulation and reactive power capabilities and is Category II for disturbance ride-through requirements.

2.2.3 General Specifications and Performance Requirements

This section of the standard first defines where the reference point of applicability (RPA) should be located, either at the PCC or at the PoC. This location is based on the size of the DER, its load demand, and the continuity of zero sequence current between the PCC and the PoC [4]. Zero sequence current refers to the unbalanced current flow in a circuit that can arise from disruptions between the two connection points (e.g. a delta-wye transformer) and ensuing system faults, which leads to a loss in measurement and detection accuracy [13]. For the microgrid used in this thesis, the RPA is located at the PoC.

The applicable voltages are defined for different types of DERs. The applicable voltage is the measured quantity at the RPA and varies based on the DER voltage level and the winding configuration of the area EPS transformer [4]. For the microgrid used in this thesis - a single-phase 120 V nominal system - the applicable voltage is the line-to-neutral voltage measured at the RPA and is quantified as the root mean square (RMS) value over one period of the fundamental frequency of the system (60 Hz) [4].

The standard defines the cease-to-energize conditions. In a cease-to-energize state, the DER does not deliver active power to the EPS at the PoC. Any reactive power exchange during this state is allowable at less than 10% of the rated system reactive power and results exclusively from passive means (e.g. an internal system cooling fan) [4]. Any import of active power from the EPS is allowed for the same purpose as reactive power.

The DER should be able to control certain functions, such as cease-to-energize, the ability to limit active power to the EPS and mode-switching. The DER should also prioritize responses in the event that multiple events occur simultaneously. The ability to cease to energize and disrupt the connection to the EPS is the top priority. The DER, when initially engaging with the EPS upon start up (otherwise known as "entering service"), must first meet an acceptable voltage and frequency range before any interaction is allowed. Upon reaching the allowable ranges, the DER must then meet synchronization criteria before connecting to the local or area EPS. Any DER system that is used for emergency purposes, as defined in the standard, is exempt from voltage and frequency ride-through disturbances, interoperability and information protocols and intentional islanding requirements [4]. As the microgrid used in this thesis does meet the description of an emergency system, all of the following sections will apply to its operation.

2.2.4 Reactive Power Capability and Voltage/Power Control

The standard requires the DER to be able to control voltage, active power and reactive power in response to voltage variations within a normal operating range (this range is specified in Section 2.2.5). The DER is also required to be able to inject or absorb reactive power for active power output that is equal to or greater than 5% of the rated active power [4].

The DER is required to regulate its voltage by changing the reactive power via four control function modes: constant power factor mode, voltage-reactive power mode, active power-reactive power mode and constant reactive power mode [4]. Each of these modes should be able to be executed exclusively of the others by the DER, and the purpose of each is to regulate the output voltage to a reference voltage that is acceptable to be synchronized with the EPS voltage. Similarly, the DER should be capable of regulating the voltage level to a reference voltage by means of controlling the active power output.

2.2.5 Response to Area EPS Abnormal Conditions

This section of the standard addresses abnormal conditions for voltage and frequency and the appropriate DER response to those conditions. The requirements in this section refer to the applicable voltages of the system at the RPA.

Abnormal Voltage Conditions

In the event of an area (or local) EPS short-circuit fault, the DER must cease to energize and disconnect from the EPS. In the event of a DER open-phase condition (for a multi-phase system), the DER must cease to energize and disconnect from the EPS within 2.0 s of the initiation of the condition [4].

For a condition of the applicable voltage being less than an undervoltage threshold, or greater than an overvoltage threshold, the DER must cease to energize the EPS and trip within a specified clearing time. Certain voltage ranges, however, allow for the DER to ride through a voltage disturbance for a range of time, as shown for Category II in Table 2.1. Should the DER trip within these allowable ranges due to its own self-protection, then it shall be considered a failure to comply with the standard [4].

Table 2.1. Voltage ride-through ranges associated with Category II DERs. Source: [4].

Voltage range (p.u.)	**Operating mode/response**	**Minimum ride-through time (s) (design criteria)**	**Maximum response time (s) (design criteria)**
$V > 1.20$	Cease to Energize[a]	N/A	0.16
$1.175 < V \leq 1.20$	Permissive Operation	0.2	N/A
$1.15 < V \leq 1.175$	Permissive Operation	0.5	N/A
$1.10 < V \leq 1.15$	Permissive Operation	1	N/A
$0.88 \leq V \leq 1.10$	Continuous Operation	Infinite	N/A
$0.65 \leq V < 0.88$	Mandatory Operation	Linear slope of 8.7 s/1 p.u. voltage starting at 3 s @ 0.65 p.u.: $T_{VRT} = 3\text{ s} + \frac{8.7\text{ s}}{1\text{ p.u.}}(V - 0.65\text{ p.u.})$	N/A
$0.45 \leq V < 0.65$	Permissive Operation	0.32	N/A
$0.30 \leq V < 0.45$	Permissive Operation	0.16	N/A
$V < 0.30$	Cease to Energize[a]	N/A	0.16

Any voltage disturbance within the continuous operation range as defined in Table 2.1 will not cause the DER to cease to energize from the EPS, and the DER shall continue to deliver active power. Temporary deviations (i.e., transient responses) not exceeding 0.5 s are allowed to occur while in the continuous operation range [4]. The allowable voltage range for continuous operation is derived from Range B voltages in American National Standards Institute (ANSI) Standard C84.1-2020, displayed in Figure 2.2.

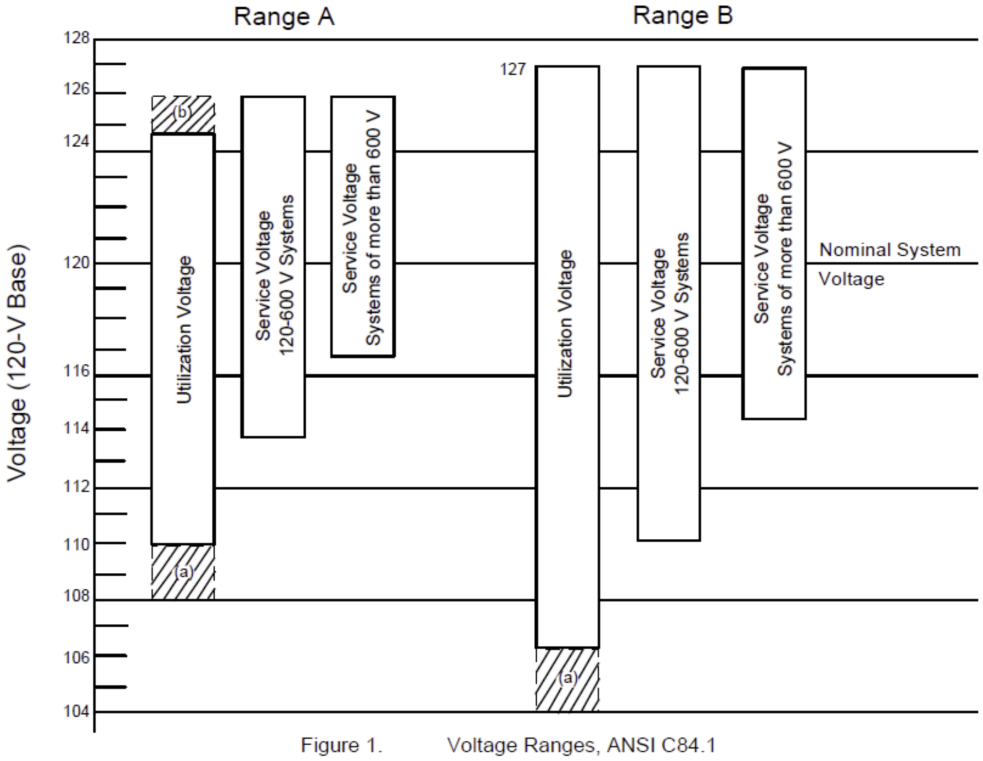

Figure 2.2. Allowable Range B utilization voltage range for IEEE Standard 1547-2018 Source: [14].

For an undervoltage event, when the applicable voltage of the DER is less than 0.88 per-unit (p.u.) and is within the mandatory operating region from Table 2.1, the DER is required to maintain synchronism with the EPS, to continue the exchange of current with the EPS and shall neither cease to energize nor trip [4].

When the applicable voltage of the DER for an undervoltage event is within the permissive operating region from Table 2.1, the DER is required to maintain synchronism with the EPS and may continue the exchange of current with the EPS or may cease to energize (either event is acceptable) [4]. These conditions are also applicable to an overvoltage event, with an applicable voltage over 1.10 p.u. but less than 1.20 p.u.

In an undervoltage or overvoltage event where the applicable voltage is in the cease to

energize operating region, the DER shall cease to energize the EPS within the maximum response time from Table 2.1. This does not imply a direct disconnection or trip from the EPS but could be satisfied with momentary cessation, where the DER remains connected to the EPS but simply ceases to energize at the RPA [4].

Once an applicable voltage has surpassed the lower value of the mandatory operating region for an undervoltage event, or has returned below the higher value of the permissive operating region for an overvoltage event, the DER shall restore the active current output to at least 80% of its pre-disturbance value within 0.4 s [4].

Abnormal Frequency Conditions

When the DER applicable voltage is greater than 30% of the nominal and the system frequency is within the ranges specified in Table 2.2, then the DER shall either cease to energize or ride through the disturbance accordingly [4].

Table 2.2. Frequency ride-through ranges associated with Category I, II and III DERs. Source: [4].

Frequency range (Hz)	**Operating mode**	**Minimum time (s) (design criteria)**
$f > 62.0$	No ride-through requirements apply to this range	
$61.2 < f \leq 61.8$	Mandatory Operation[a]	299
$58.8 \leq f \leq 61.2$	Continuous Operation[a,b]	Infinite[c]
$57.0 \leq f < 58.8$	Mandatory Operation[b]	299
$f < 57.0$	No ride-through requirements apply to this range	

For frequency disturbances within the continuous operation region from Table 2.2, given that the p.u. ratio of voltage-to-frequency is less than or equal to 1.1, the DER shall not trip but shall ride through and continue to operate [4]. For both low and high frequency disturbances within the mandatory operating region from Table 2.2, having a duration less than 300 s within any ten-minute period, the DER shall maintain synchronism with the EPS with a continued pre-disturbance current and shall neither cease to energize nor trip. At a

frequency disturbance greater than 62.0 Hz or less than 57.0 Hz, the DER shall cease to energize the EPS [4].

2.2.6 Power Quality

This section of the standard provides limitations on rapid voltage change and current distortion for the interconnection between the DER and the EPS.

For a low voltage system (operating at less than 1 kV), the DER shall cause neither step changes in the EPS RMS voltage exceeding 5% of nominal nor ramp changes exceeding 5% of nominal per second averaged over a period of one second. These limits do not apply, though, for infrequent events, such as source switching, unplanned tripping or fault returning [4].

The DER is limited in the allowable total rated-current distortion at the RPA, according to the values in Figure 2.3. These limitations do not apply when the DER is disconnected from the EPS.

Maximum odd harmonic current distortion in percent of rated current (I_{rated})[a]

Individual odd harmonic order h	$h < 11$	$11 \leq h < 17$	$17 \leq h < 23$	$23 \leq h < 35$	$35 \leq h < 50$	Total rated current distortion (TRD)
Percent (%)	4.0	2.0	1.5	0.6	0.3	5.0

[a] I_{rated} = the DER unit rated current capacity (transformed to the RPA when a transformer exists between the DER unit and the RPA).

Maximum even harmonic current distortion in percent of rated current (I_{rated})[a]

Individual even harmonic order h	$h = 2$	$h = 4$	$h = 6$	$8 \leq h < 50$
Percent (%)	1.0	2.0	3.0	Associated range specified in Table 26

[a] I_{rated} = the DER unit rated current capacity (transformed to the RPA when a transformer exists between the DER unit and the RPA).

Figure 2.3. Limitations on rated-current distortion. Source: [4].

2.2.7 Other Requirements

The standard includes limitations and requirements of the DER for other aspects of connection.

When an unintentional island occurs for a DER that is connected to an EPS, the DER shall detect the island and cease to energize the EPS within 2 s of detection [4]. For intentional island events, either scheduled by the EPS operator or unscheduled (resulting from DER or EPS detection of abnormal condition events), the DER shall cease to energize the EPS and will conform to the rapid voltage change conditions from Subsection 2.2.6.

A DER shall be capable of remote communication to support information exchange requirements via an interface. The information to include in this exchange is the following: nameplate information of the DER system, configuration information (indicates present DER capacity and ability to perform functions), monitoring information (indicates present operating conditions of the DER) and management information (regarding the ability to update or change mode settings of the DER) [4].

The standard includes some communication protocol requirements that apply only to the local DER interface - networks outside of the DER and internal to the DER are not included. The communication interface of the DER, though, is required to be active and responsive when in a continuous or mandatory operating region, as specified in Section 2.2.5. The standard does not mandate specific cyber security requirements for the DER but recognizes the critical nature of security for information exchange and remote functionality [4].

THIS PAGE INTENTIONALLY LEFT BLANK

CHAPTER 3:
Microgrid Experimental Setup

A mobile COTS microgrid was used that can operate in an islanded state, disconnected from the local EPS, or in a grid-connected state if the local EPS is available. This chapter details the microgrid testbed, COTS components and measurement instruments used. Each component and instrument is examined to provide relevance to the experimental testing methodology. Table 3.1 contains a list of the characteristics that were experimentally tested for compliance to IEEE Standard 1547-2018 and other tested characteristics unrelated to the standard. This table provides the reader an understanding of what is to be tested so that the explanation of the system components in the testbed has relevance when discussed later.

Table 3.1. Summary of microgrid characteristics tested and analyzed

Characteristic	**IEEE Related**	**Primary Components**	**Primary Instrument**
Battery Charge	No	Battery bank PV array Charge controller	Fluke 434
Ride-Through	Yes	Power converter AC source AC load	Fluke 434
Transients	Yes	Power converter AC source AC load	Oscilloscope
Distortion	Yes	Power converter AC source Control system	Fluke 434
Power Balance	No	Battery bank AC source and load PV array	Control System

3.1 System Overview

A block diagram of the microgrid system used in this thesis is displayed in Figure 3.1 and includes the following COTS components:

- a DC power source (an array of PV panels for this system),
- a charge controller for the generated DC power,
- a battery bank for energy storage,
- a power converter to convert DC power to AC power or AC power to DC power,
- a control system with a user interface,
- AC power sources (either the local or area EPS or a generator),
- any attached loads that use the system AC power.

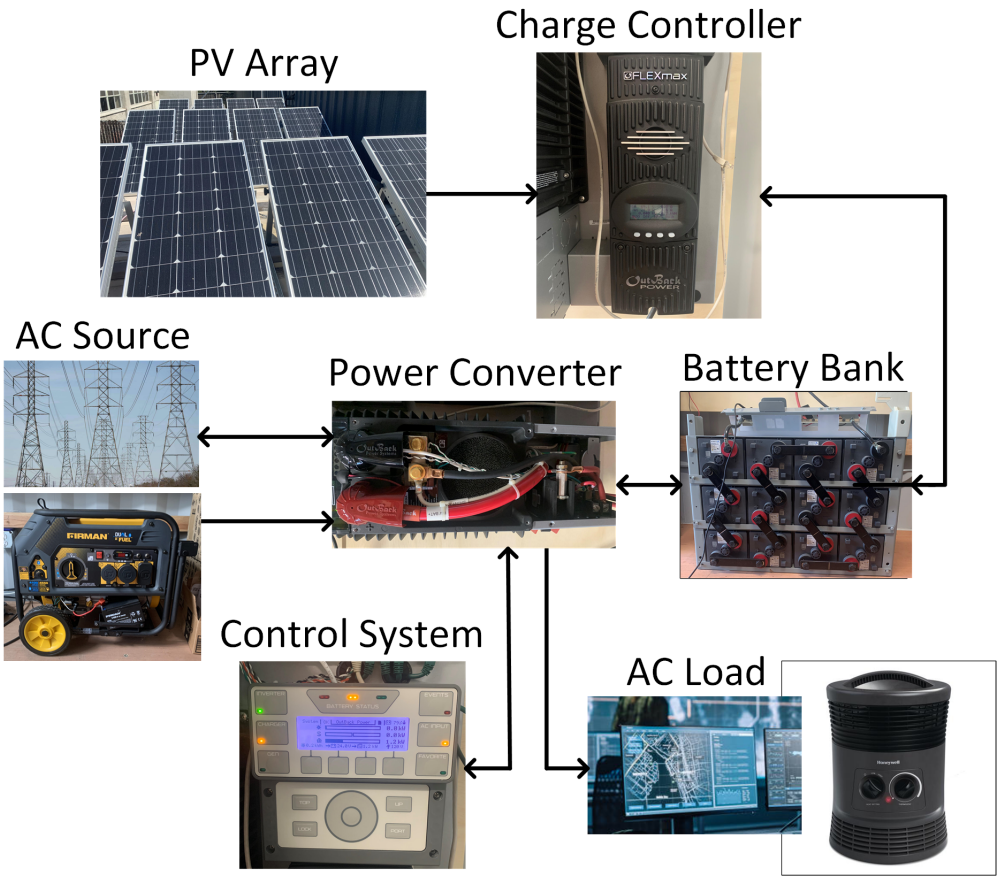

Figure 3.1. Block diagram of the microgrid system used in this thesis. The microgrid consists of seven COTS components. Image sources: [15] [16] [17].

When the microgrid is operating in islanded mode, the solar power generated flows from the PV arrays of solar panels into the charge controller and then to the battery bank. The power converter receives the power from the battery bank and converts it to AC power that is then delivered to the loads. When the loads draw too much energy from the battery bank, such that the battery state of charge (SOC) decreases to a pre-determined threshold, then the power converter switches the source of AC power to either the local grid or the generator. Alternatively, when the battery SOC is too low and the AC source switches, the microgrid will begin to supply DC power to the batteries, through the PV arrays and/or the local EPS. The microgrid power flow is clarified by the circuit schematic in Figure 3.2.

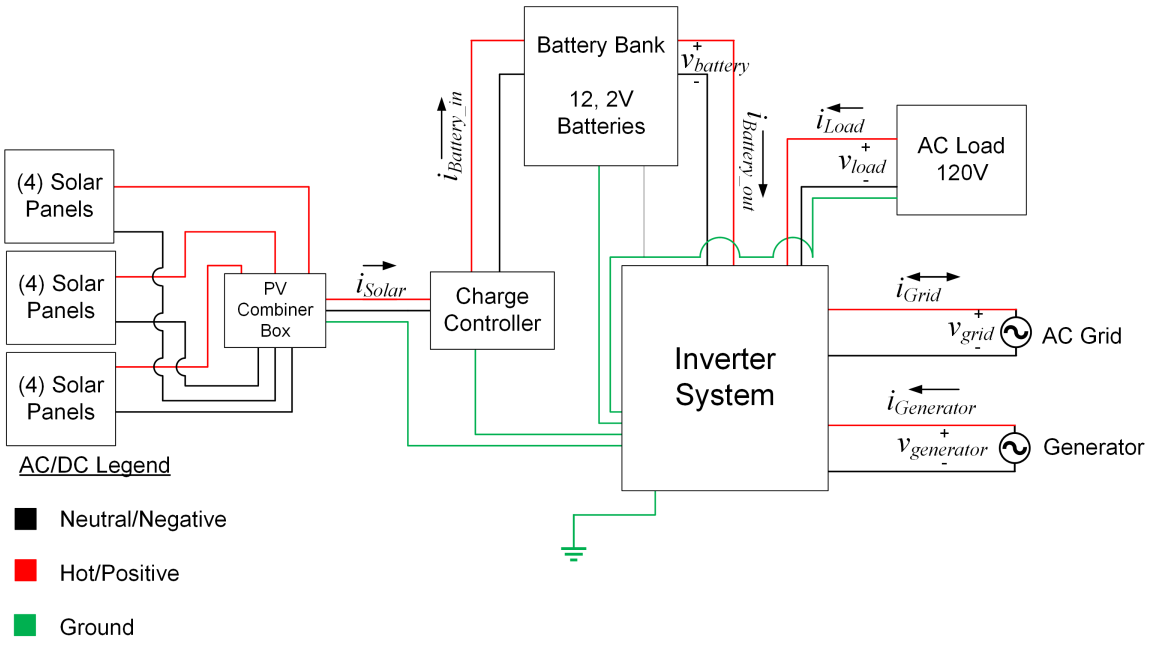

Figure 3.2. Microgrid circuit schematic.

3.2 PV Arrays

Energy from the sun is captured by a PV array in the form of solar radiation. Sunlight passes through the atmosphere and can be scattered, absorbed and reflected before reaching the surface of the Earth. As such, the condition of the atmosphere on any given day has

a significant effect on the amount of solar radiation captured by the PV array. Certain conditions have the ability to reduce the amount of radiation by nearly 100% [18]. This captured energy is the primary renewable energy source used in this microgrid and in many others. Ensuring that the PV arrays are properly arranged so as to maximize the amount of solar radiation received is critical to efficient operation. For this microgrid, the solar panels depicted in Figure 3.3 are arranged on the roof of the shipping container that is used as the microgrid testbed. The use of this shipping container and the ability to arrange the PV arrays so as to effectively capture solar radiation highlights the mobility of this microgrid. The PV arrays are arranged in three parallel strings of four panels in series.

Figure 3.3. The 12 solar panels used at this microgrid provide 1.2 kW of power.

Each of the 12 panels is rated for 12 V and is able to generate up to 100 W. The three parallel strings of four panels in series can each create 400 W (for a total of 1200 W) of power at

48 V that is delivered to the charge controller. The three strings of panels combine into one deliverable power source through the combiner box, shown in Figure 3.4. There is a breaker switch included in the combiner box that provides the ability to shut off solar power to the inverter system.

Figure 3.4. The three strings of four solar panels in series are combined into one power source through the combiner box.

3.3 Charge Controller

Each battery in the bank of batteries used in the microgrid setup is rated for 2 V. Twelve batteries combined in series provide a nominal voltage of 24 V, but the incoming voltage from the solar panels is targeted to be 12-24 V higher than the nominal [19]. This target voltage is accomplished by connecting four PV panels in series that provide 48 V to the charge controller. In order to not overcharge the batteries and cause damage to them, the voltage delivered by the PV arrays must be decreased to a lower voltage by a step-down DC-DC converter which is included in the COTS component shown in Figure 3.5, the charge controller.

Figure 3.5. The charge controller's primary goal is to maximize the incoming solar power and convert it to a nominal level for the batteries.

Although the combined rated power of the PV arrays is 1200 W, the realistic amount of power drawn is less. However, the power from the PV panels is always desired to be at a maximum output level, and the charge controller uses maximum power point tracking (MPPT) technology to ensure this. Figure 3.6 displays the relationship between the voltage and current delivered to a load, which when multiplied together provide the active power. The available power is shown with the maximum power (MP) point highlighted. The charge controller provides its own variable load to the PV array in order to track the voltage and determine where the maximum power point is for any given atmospheric situation. Upon sensing where that MP point is, the charge controller locks onto that load and supplies the maximum available power to the batteries.

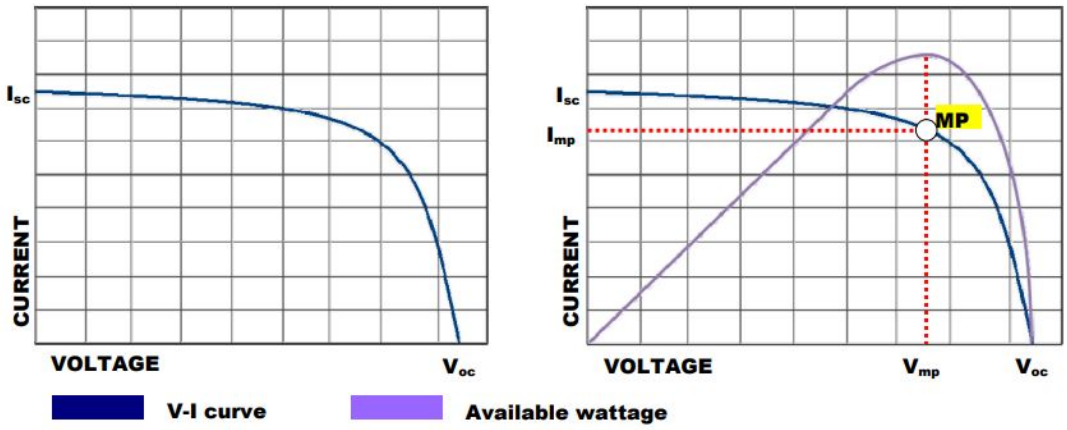

Figure 3.6. MPPT provides a constantly optimal voltage point to obtain the maximum available power from the PV arrays. Source: [19].

The charge controller uses the MPPT function in conjunction with a multi-stage charging setup that provides the maximum charging capacity for the batteries based on the time of day and the amount of solar irradiance available. The three main stages of this process are bulk charging, absorbing and floating, as defined by the manufacturer and shown in Figure 3.7. The battery and PV array voltages in Figure 3.7 are associated with the charging stage of the controller.

When in the bulk charging state, the charge controller provides a constant current to the

batteries which drives an increased voltage to the batteries. In this stage, the batteries are increasing charge and are "bulking" in order to provide required power for the daily load profile. The end state of this stage leaves the batteries typically between 75% to 90% SOC, but the absorbing voltage is the target. Once this absorbing voltage has been achieved, the charge controller moves on to the next stage. In the absorbing stage, the charge controller provides the batteries with a constant voltage and a varying current that enables the controller to maintain the absorbing voltage in the batteries. Slowly, the battery SOC will continue to increase until it reaches approximately 100%. After a scheduled time in this stage, the charge controller will exit the absorbing stage and move forward into the float stage. The float stage maintains the battery voltage and SOC at a specified value until the available solar power is unsustainable to maintain that value, at which time the charge controller has the ability to launch another cycle of battery charging [19].

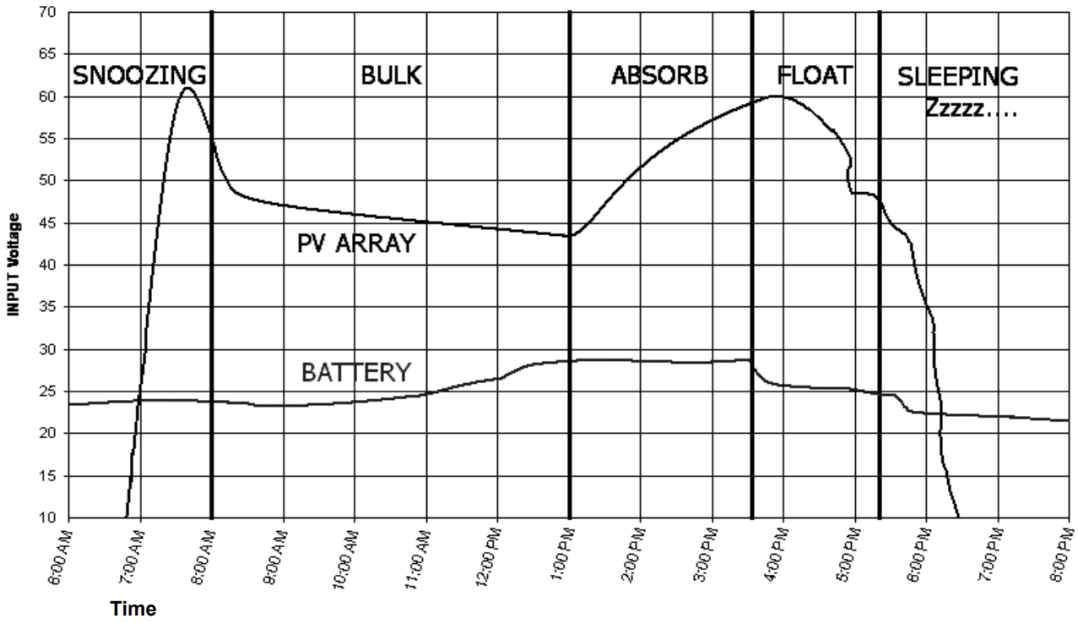

Figure 3.7. The charge controller provides maximum charging power to the batteries through the MPPT function, according to the solar irradiance present during a typical day. Source: [19].

3.4 Battery Bank

The discharge and recharge of an energy storage component is an important function of a microgrid. For this microgrid testbed, the battery bank shown in Figure 3.8 is the energy storage component. This bank consists of 12 2-V batteries in series (creating a 24 V nominal output) that are rated for 500 Ah for 10 hours and for 5000 life cycles at a 70% depth of charge (down to 30% SOC) [20]. Each of these batteries is composed of several chemical compounds (e.g. lead-acid, lead-carbon, nickel-cadmium, lithium-ion [20]) that allow current (from either the charge controller or from the power converter) to flow into the batteries which reverses the chemical ionization in the electrolyte, thus allowing the batteries to recharge [21].

Figure 3.8. The batteries used in the microgrid setup include 12 2-V lead-acid (primary compound) batteries in series.

Referring to Figure 3.2, the current flowing from the batteries to the power converter is positive when the battery bank supplies energy and negative when the battery bank is being charged. When the SOC of the batteries draws down to a determined level, the batteries will cease to supply DC power to the power converter (thus, the load) and will instead absorb power from both the PV panels and from the active AC source until a higher threshold SOC has been reached. This, in effect, minimizes the amount of power drawn from the grid and utilizes the stored energy in the batteries to power the loads.

3.5 Power Converter

This power electronics system provides bidirectional power conversion capability. It converts DC power from the batteries into AC power that is used by the loads, and it also converts AC power from the active AC input source (local EPS or generator) to DC power that charges the batteries. The DC to AC conversion is accomplished with a high-frequency h-bridge inverter to convert the power and a transformer to boost the power to the appropriate level used by the loads [22]. This system uses the same h-bridge inverter when converting AC power to DC, making it bidirectional, and then steps the voltage down to an acceptable level for the batteries. The schematic of a typical h-bridge inverter circuit is shown in Figure 3.9. The inverter in this microgrid testbed receives the DC voltage from the batteries as an approximately constant value and regulates the magnitude and frequency of the single-phase output AC voltage to 120 Vrms at 60 Hz, through control of the switching semiconductor gates [23]. When the power flow reverses, the inverter converts the AC voltage to DC to charge the battery bank.

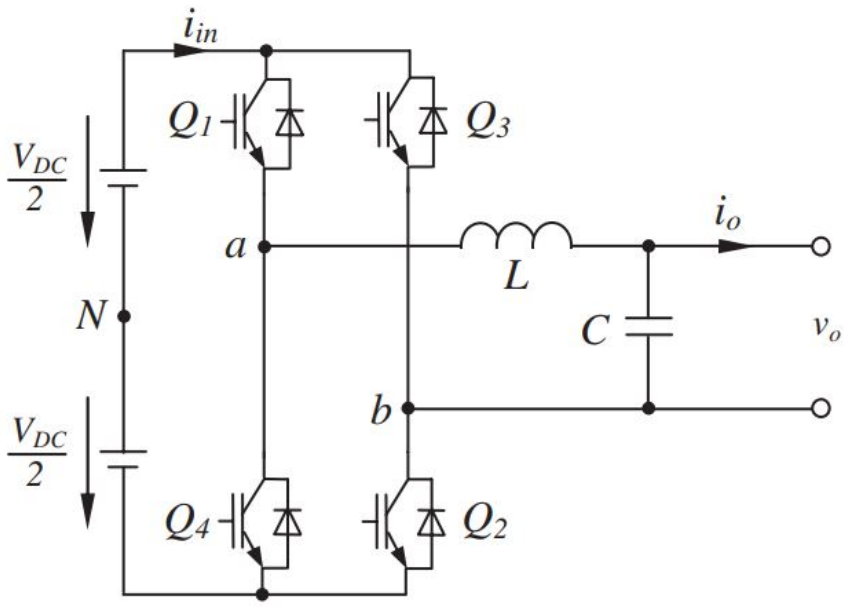

Figure 3.9. This bidirectional power converter circuit is used to interface between the battery DC bus and the AC bus where the loads are connected. Source: [24]

The COTS power converter, shown in Figure 3.10, forms the AC bus when the microgrid operates in islanded mode. It has the following seven operating modes for AC output generation, each with a unique set of capabilities and limitations [22]:

- Generator - used for generators and other irregular AC sources
- Support - power converter used to support the AC source
- Grid-Tied - creates a grid-interactive relationship between the local EPS and the power converter
- Uninterrupted Power Supply (UPS) - provides the fastest AC source switching time
- Backup - power converter used in the event of a grid failure
- Mini-Grid - disconnects from the local EPS until the batteries are too low
- Grid-Zero - remains connected to the local EPS but zeroes EPS usage

Figure 3.10. This COTS power converter from Outback Power is used in the microgrid testbed to provide multiple operating modes that optimize AC source usage and maximize renewable energy usage. Source: [22].

Generator mode allows for a wide range of AC source input variability. Some self-excited sources may initially produce voltages with highly distorted waveforms at frequencies that do not match the power inverter output. These sources can still be accepted by the power converter with a delay time that allows them to self-regulate to the appropriate frequency. Other sources may not need that delay time to be able to produce voltages at an acceptable frequency, but the voltages they produce might have greater harmonic distortion, which could lead to a potential deviation from IEEE Standard 1547, as discussed in Section 2.2.5. This operating mode, for the power converter, takes into account the possibility for harmonic distortion and frequency abnormality and is able to process these input sources to be able to provide an appropriate output voltage to the load. However, because of the possibility for abnormalities in the voltage, this operating mode does not allow for

exporting or selling power back to the AC source. Additionally, “any AC fluctuations that are accepted by the inverter will be transferred to the output. The loads will be exposed to these fluctuations” [22]. This mode, therefore, might not be appropriate for sensitive loads. This mode does not require that a generator be connected to the power converter, nor does it require that this mode be selected when the power converter is connected to a generator.

In support mode, the primary power source is either the local EPS or a generator, and the power converter supplies power via the batteries when it is required. When a threshold grid or generator input AC limit has been exceeded by a large load demand, then the power converter will support the loads with the battery power. However, when this condition arises and the system supports the loads with battery power, the battery SOC will continue to drain unless the solar power from the PV arrays is greater than the output power supplied by the batteries. Alternatively, when the DC power generated from the PV arrays is greater than the load demand, then the excess power will be used to offset the AC source. In this mode, the battery storage capacity is conserved and is only used for large load demands.

The main feature of grid-tied mode is the ability to sell excess power to the utility grid. In this mode, the power converter uses the local EPS as the primary power source and maintains a maximum SOC in the batteries. Similar to support mode, excess DC power generated by the PV arrays can be used to offset the load demand, but if there is any excess DC power beyond what is required by the loads, then that excess power is sold to the utility grid. This mode maximizes the battery SOC and will only disconnect from the local EPS if there is a trip in the system, as defined in Section 2.2.5, or if the local EPS is disconnected.

In UPS mode, the power converter provides continuous power to the load with the fastest transfer time when shifting between AC sources or when there is a local EPS failure. This mode is optimal for sensitive loads that require an uninterrupted power supply. However, because of the need for the power converter to actively monitor the AC source for disturbances, this mode requires a continuous consumption of 42 W. This has little effect on the total load demand, as the effective maximum sustainable load output is reduced from 3.5 kVA to 3.45 kVA.

In backup mode, the power converter is only used when the local EPS is disconnected or tripped. At that time, the power converter will supply the loads with power from the battery

bank until the local EPS is restored. The grid power will then simultaneously be used to power the loads and to recharge the batteries. The benefit of this operating mode is that the battery SOC is always at a maximum capacity, given the full time to recharge. This mode will not use excess power from the DC source to offset the loads.

In mini-grid mode, the power generated by the DC source is the primary power supply. The AC source is only used when the battery voltage reaches a disconnect threshold. When the battery voltage is depleted to that value, the power converter will switch to the AC source to supply power to the loads. The AC source can also supply power to the batteries for recharging, or the system can be set to have the renewable energy source be the primary recharging source for the batteries. Once the batteries have reached a reconnect voltage threshold, the power converter will disconnect from the AC source and will once again service the loads only from the DC power source. This operating mode is optimal for a location with a larger renewable energy source available, as it relies on this power source to minimize the AC source usage.

In grid-zero mode, the power converter maintains its connection to the AC source (primarily using the local EPS as the source) but minimizes this source usage by prioritizing the use of the batteries to provide power to the loads. As the battery voltage decreases to a specified threshold, the flow of power to the loads will also decrease (but not cease) so that the power converter maintains the batteries at that threshold voltage. The AC source is only utilized when that threshold voltage is reached, at which point the AC source will supplement power to the loads while the renewable energy source charges the batteries. The power converter does not charge the batteries from the AC source in this mode. Because of this, this mode is only optimal when there is a large supply of renewable energy that exceeds the energy demand of the loads.

The multiple modes of operation for the power converter provide options for an optimized microgrid setup, based upon load profile, the types of loads used and the environmental situation.

3.6 Control System

The control function for this microgrid testbed is performed by the Mate3s interface from Outback Power. While the system can run without this active control program, enabling its display and features allows for multiple operating modes that are appropriate for varied environmental situations and desired loads. Mate3s has control capability, through an Ethernet port hub shown in Figure 3.11, of the power converter and its connections to the batteries, the charge controller, the AC sources and the loads. Two features, separate from the operating modes mentioned in Section 3.5, will be highlighted for their relevance to the experimental setup.

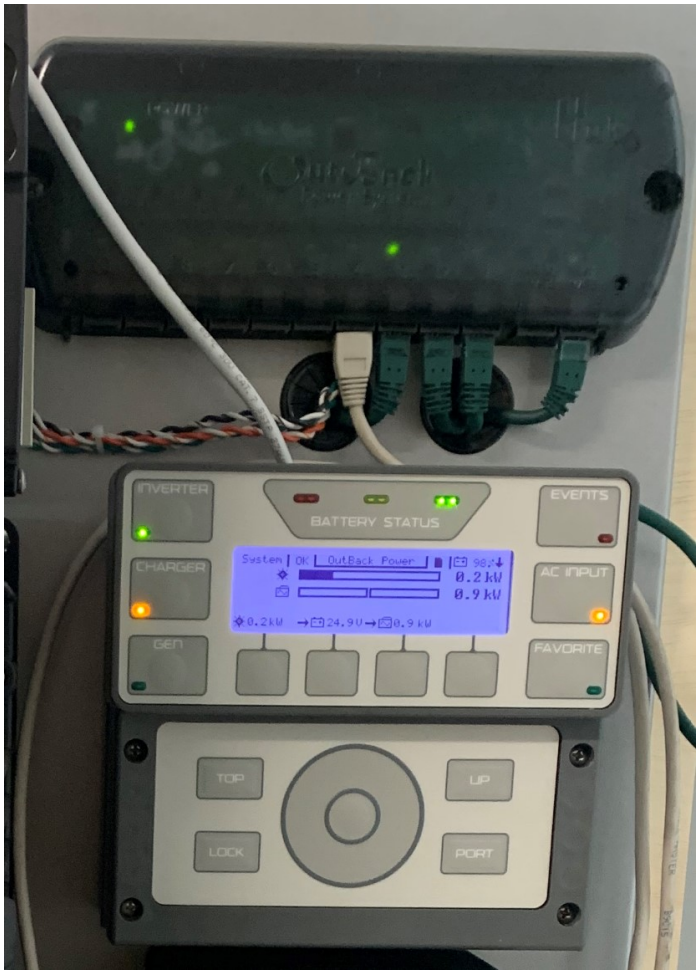

Figure 3.11. This microgrid is controlled through the Mate3s control system from Outback Power.

High Battery Transfer (HBX) is a feature of the system that is controlled through Mate3s. It is not an operating mode on its own but can be used in conjunction with other microgrid modes of operation. HBX enables the system to draw down the batteries to a lower threshold SOC or voltage and then switches to the local EPS as the primary AC input source. After this switch, the batteries are charged to an upper threshold SOC or voltage, and then the AC source again switches to the power converter, using the battery power. This operation differs from the mini-grid operating mode in that the SOC can be used as the threshold value rather than the battery voltage. For this reason, the system cannot operate in mini-grid mode and in HBX, but any other operating mode accepts this feature.

The search function provides the system the ability to minimize inherent power usage while retaining the ability to operate loads as required. In this function, the power converter only provides AC power in small pulses, with a delay between each pulse, that either meet a load resistance or not. Based on that search for a load, the system is able to operate in a low-power mode that enables it to maintain residual power for a longer period of time [22].

In addition to the physical changes that can be implemented at the Mate3s interface, this microgrid system also has remote operation capability through the OpticsRE program from the Outback Power website. The operations that are able to be affected from OpticsRE are limited, but they have the potential to provide a significant impact to the continuous function of the loads. Figure 3.12 displays the standard view of information that is presented with OpticsRE. Through this remote interface, the user is able to view system data from the present day or any day from the previous five years.

Figure 3.12. OpticsRE provides the user of this microgrid the ability to view and control certain functions from a remote location.

The OpticsRE remote control program has the ability to alter certain functions of the microgrid. The functions shown in Figure 3.13 indicate that the user has the option to change the charge controller charging status and has the ability to turn on or off both the power converter and the AC input source (either the generator or the local EPS). This gives rise to a threat on the system - should an attack be made and the remote system interface be accessed, the ability to control some of the system parameters is at jeopardy. The bulk charge status can be affected to either overstimulate or drain the battery voltage such that it might not be capable of providing adequate power to the loads in the event of a grid or generator failure. That sort of AC source failure could also result from an unwanted shut-off from the same attack. Turning off the inverter on its own has no effect on the loads while the AC source is actively operational, but upon that failure or switch, the inverter will cease to provide power to the loads, forcing them off.

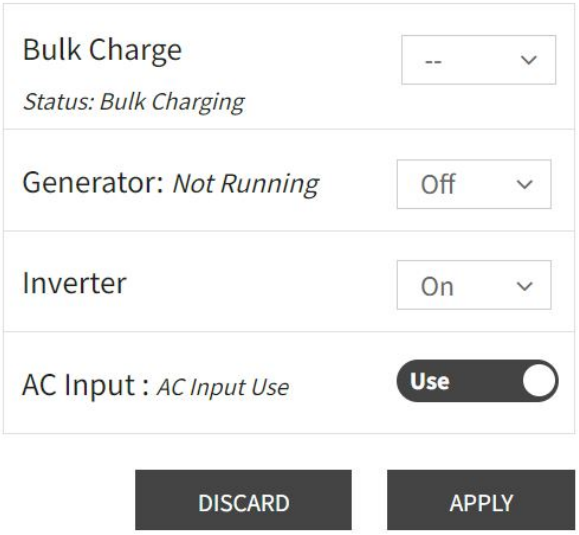

Figure 3.13. Within the OpticsRE program, the user has the ability to affect the main microgrid components and functionality.

OpticsRe is not a mandatory tool for this microgrid system to be fully operational. It can operate without remote access through controls taken with Mate3s. However, in the event that this remote program access is used, being able to provide security for the operations is critical for the success of the system.

3.7 AC Loads

The loads used to test this microgrid were a combination of three COTS space heaters. These heaters each draw a relatively high amount of power when activated which allows the microgrid to be tested at a larger percentage of the rated load. The heaters consist of heavily resistive coils (to produce heat) and a small motor for the fan. The combination of these electrical components enables the heaters to draw mostly active power but also some reactive power. The reactive power drawn by the small motors is less than 2% of the rated total power and is not significant enough to be included in the results of this thesis. Two of the three heaters have low-power and high-power settings, which enables a variation of loads to be placed upon the system. This allows the microgrid characteristics to be tested at

different load demands to observe the variations in responses. The information provided in Table 3.2 shows the rated power and current for the three different heaters. Each current is calculated by dividing the rated power by the standard EPS voltage, 120 V.

Table 3.2. Three loads were used in this thesis with different power demands.

Heater	**Low Power Rating (W)**	**Low-Power Current (A)**	**High Power Rating (W)**	**High-Power Current (A)**
1	500	4.17	900	7.5
2	N/A	N/A	1200	10
3	750	6.25	1500	12.5

3.8 Measurement Instruments

In order to properly examine and test this microgrid system for its characteristic parameters, functionality and its compliance with IEEE Standard 1547, several measurement instruments were used. The two primary instruments used were the Tektronix Mixed Signal Oscilloscope 4034 (hereafter referred to as, "oscilloscope") and the Fluke 434 Power Quality Analyzer (hereafter referred to as, "Fluke 434"). Both have abilities that allow specific microgrid characteristics to be measured, and both will be highlighted.

The oscilloscope, shown in Figure 3.14, is a four-channel measurement instrument that is used in this experimental setup to capture the source and load currents and voltages. Data captured includes voltage and current transients, delay times, RMS values for load voltage and current and local AC grid current.

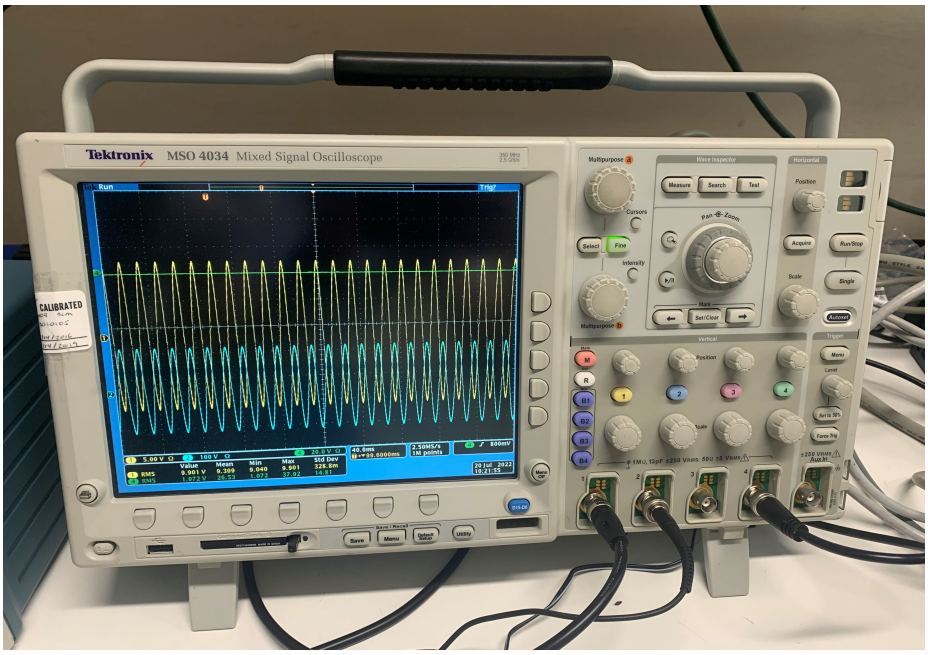

Figure 3.14. The Tektronix Mixed Signal Oscilloscope 4034 measurement instrument is used to monitor and capture current and voltage waveforms.

The Fluke 434, shown in Figure 3.15, is a power quality analyzer that has multiple capabilities. In this experimental setup, the Fluke 434 is used to monitor and capture data such as load voltage and current, harmonic distortion, active, reactive and apparent power, power factor, voltage transients and current transients.

Figure 3.15. The Fluke 434 Power Quality Analyzer measurement instrument is used to monitor and capture voltage, current, power and frequency information, among other characteristic parameters.

Both the Fluke 434 and the oscilloscope provide unique capabilities for the research in this thesis. The oscilloscope is able to capture instantaneous data for voltages and currents, down to nanosecond resolution, which is critical for observing and understanding system transient responses. The Fluke 434 is able to provide long-term monitoring of multiple data sets that allows for several parameters to be observed at the same time, for the same experimental trial. The utilization of these instruments together, in coordination with the operating modes and other features of the Outback Power system, provides an appropriate setup for the testing and characterization of the COTS microgrid.

3.9 Summary

This chapter has provided an overview of the component structure of the microgrid testbed used in this thesis. Understanding the structure of each component enables a better view of the microgrid as a whole and provides insight as to how the relationships between certain components will be displayed. These relationships will be tested and examined for compliance to IEEE Standard 1547-2018.

CHAPTER 4:
Experimental Testing

This chapter includes the testing methodology, results and analysis for each desired characteristic of the microgrid. A characteristic, in this thesis, is a parameter of the system for which information is required so as to determine the system capabilities and limitations for the purpose of supporting a sensitive load or loads. Each section of this chapter highlights a different characteristic and includes why it is an important parameter to understand as well as the methodology of each test, the results and analysis of those results.

Although not every characteristic has a corresponding connection to IEEE Standard 1547-2018, each is important in determining the functionality of the system as it relates to providing adequate power to the loads. It should also be noted that this microgrid was tested using several AC resistive loads. This has no effect on the values of the output voltages and currents measured for the load, but the effects of system transient responses and overvoltage/undervoltage ride through capabilities may be different for more inductive versus resistive loads or for DC versus AC loads.

4.1 Battery Discharge/Recharge

A primary function of a microgrid is to be able to provide power to the loads in an islanded operating state, when disconnected from the local EPS or alternative AC power source, using the stored power in the ESS. However, the ESS power storage level decreases with time unless the power generated from the renewable energy source(s) is greater than the load demand. Once a critical-low threshold has been reached for the ESS, the microgrid will need to switch back to the local EPS or alternative AC power source in order to draw power for both the loads and to recharge the ESS. It is important to understand how long the system can operate in an islanded state in order to appropriately plan how to run a series of loads, with different demand ratings. The time and condition of the day for which the loads are running also factor into this planning. For example, solar irradiance has an effect on the PV array capability to produce DC power, so running a series of loads with PV arrays as a DC power source would be more appropriate on a sunny day than a cloudy one. However,

loads cannot always be scheduled according to the time and condition of the day, so it is equally important to know how the system will operate in various environmental conditions.

Additionally, once the microgrid has switched back to the local EPS or alternative AC power source, it is important to understand how long it will take for the ESS to fully recharge. The load demand and time/condition of the day all factor into this recharging capability and should be considered when planning for energy use/consumption (e.g. power drawn from the local EPS or fuel used by a generator) over a period of time.

A test was conducted to examine the ESS capability of discharge and recharge. For this microgrid, the ESS component is the battery bank. The test was conducted over a 24-hour period of time (beginning at 0830 h on a given test day) and compared the battery discharge/recharge times for different percentages of the rated load. The battery discharged in an islanded operating state and recharged once the system reconnected to the local EPS. The rated load for this COTS system is 3.5 kW [22], and the system was tested at 20%, 40% and 60% of the rated load in order to observe the effects that different load demands have on the battery SOC. Table 4.1 displays the testing conditions and experimental trials.

Table 4.1. Experimental Trials for Battery SOC.

Experiment#	% of Rated Load	Load Value (W)
1	20	700
2	40	1400
3	60	2100

The SOC is the measured metric for this test, as it indicates the battery capacity over time. Each test was conducted in the backup operating mode (reference Section 3.5) for consistency in testing, under the HBX system function, which enabled control of the SOC low and high threshold values of 60% and 95%, respectively. The data generated for this test came from OpticsRE, explained in Section 3.6. OpticsRE also has a data-collection function that continuously obtains and uploads multiple data sets, while connected to the

internet, at 15-minute intervals. The SOC profiles, displayed in Figure 4.1, were generated from 15-minute interval data points for the different load demands.

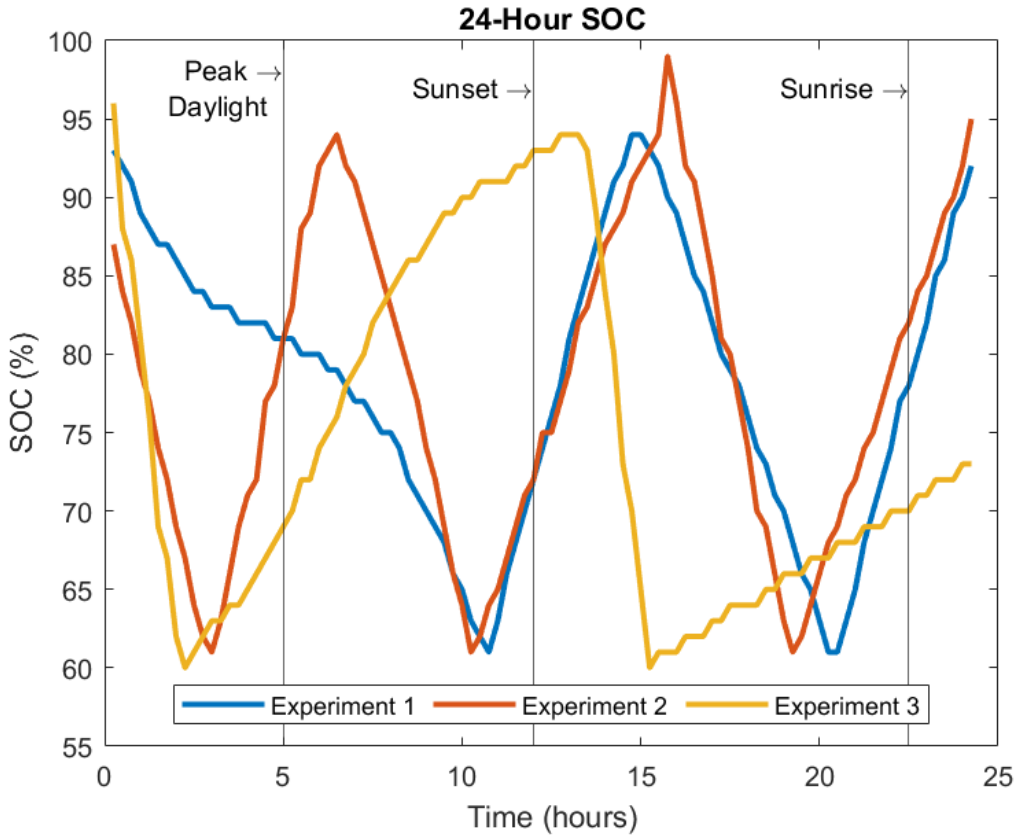

Figure 4.1. 24-hour SOC discharge/recharge trials for three separate loads

The ability of the microgrid to sustain a load and maximize the SOC varies with the solar irradiation present during a given day. As the sunlight more directly impacts the PV array, the amount of energy absorbed by the panels provides increased power to the microgrid. The solar irradiation profiles for Monterey, CA during the experiments are provided in Figure 4.2, which shows the irradiation over the 24-hour testing duration. The irradiation, when compared with the SOC profiles in Figure 4.1, illustrates the capability of the microgrid to sustain a load in an islanded state.

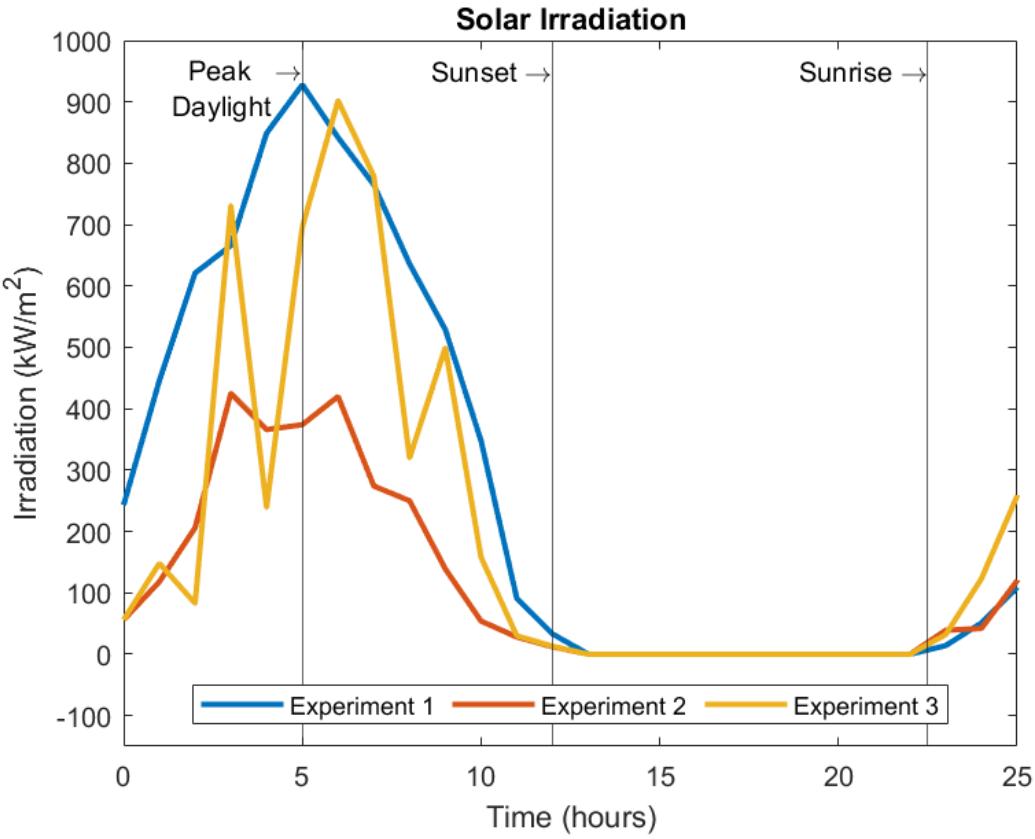

Figure 4.2. Solar irradiation profiles during each battery discharge/recharge test. Source: [25].

When there is no direct sunlight to provide DC power to the batteries through the PV arrays, the only input power is from the AC source. During these times, the time to recharge the batteries is slower than when exposed to higher solar irradiation. It can be observed from Figures 4.1 and 4.2 that this concept is true for the 2100 W load, as the time to recharge increases significantly after the daylight hours are over. It is also observable that the battery discharge times are similar for all three loads during non-daylight hours, indicating consistency of discharge for the microgrid when in an islanded operating state. The total time spent in an islanded operating state versus a grid-connected state is critical for energy planning. The microgrid was in an islanded state for 66% of the time during Experiment 1, 42% during Experiment 2 and 14% during Experiment 3. Understandably, these figures indicate that for this COTS microgrid, the battery SOC is significantly affected

by the time of day of operation as well as by the load demand on the system.

4.2 Voltage and Frequency Ride-Through

In the event that a system experiences a surge of electricity, either through natural occurrences (e.g. a lightning strike) or through man-made occurrences (e.g. stepping a load to a higher or lower output level or switching between AC input sources), it is critical that that system rides through that surge to protect the continuity of power to the loads or ceases to energize in order to not overheat any system component, causing irreparable damage. This surge produces a current spike in the system that can drive the voltage and frequency over or under their respective nominal values, creating either an overvoltage/undervoltage or an overfrequency/underfrequency that the system must then ride through in order to maintain compliance with IEEE Standard 1547-2018, provided in Section 4.2.

To test the voltage and frequency ride-through capacities of this microgrid system, several experiments were conducted for the four following operating modes (as defined in Section 3.5): Backup, Grid-Tied, Support and UPS. Of the seven, these four modes were chosen because of their practicality when operating with a primarily grid-connected microgrid. Two tests were conducted on the microgrid to evaluate the ride-through capabilities. The first test involved stepping the load to higher or lower values during a constant AC input condition, while the second test involved switching the AC input source for a constant load of 1200 W.

4.2.1 Step-Load Test

The first test began with a 500 W load that was then stepped to 1700 W, 1200 W and 2100 W, each with a two-minute interval of operation to allow a steady-state condition to be reached. Each operating mode was used in both grid-connected mode and in islanded mode, and the voltage and frequency profiles were monitored for compliance with the standard for the load changes. Figures 4.3 - 4.6 display the voltage and frequency profiles in both the grid-connected and islanded operating states.

During the operation of the grid-connected test, the 2100 W load drew a current that slightly exceeded the capability of the 20 A breaker that connects the EPS to the microgrid,

resulting in failures that can be observed by immediate voltage drops just after 6 min for backup mode and at 7.5 min for UPS mode. This also occurred in an islanded operating state for backup and grid-tied operating modes, because those two modes remain connected to the EPS regardless of the fact that the active power draw from the EPS is zero. Figure 4.3 shows that the microgrid operates closest to nominal voltage in the support operating mode, when grid-connected, and the voltage when stepping between loads is nearly the same for backup and grid-tied operating modes. Figure 4.4 shows that the voltages remain relatively consistent regardless of the operating state. Figure 4.5 shows that the operational frequency remains just slightly under the nominal for each operating mode when grid-connected, and Figure 4.6 shows that the frequency is essentially the nominal for any operating mode in an islanded state.

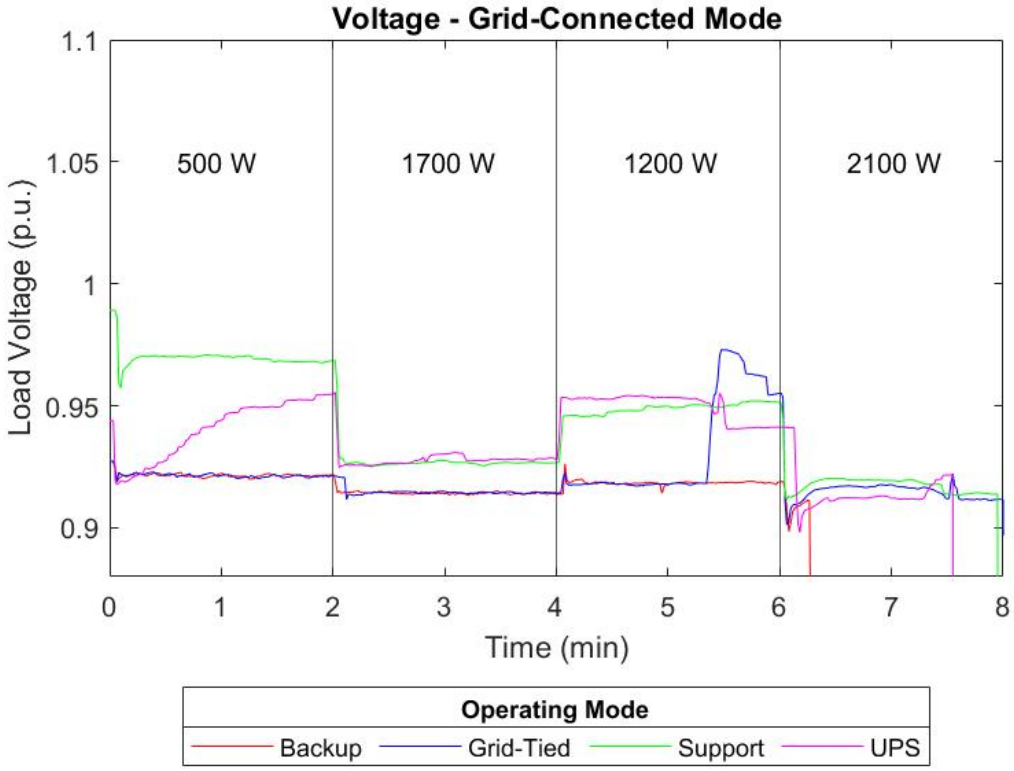

Figure 4.3. The load voltage profiles of each operating mode for the given step-load test in grid-connected mode.

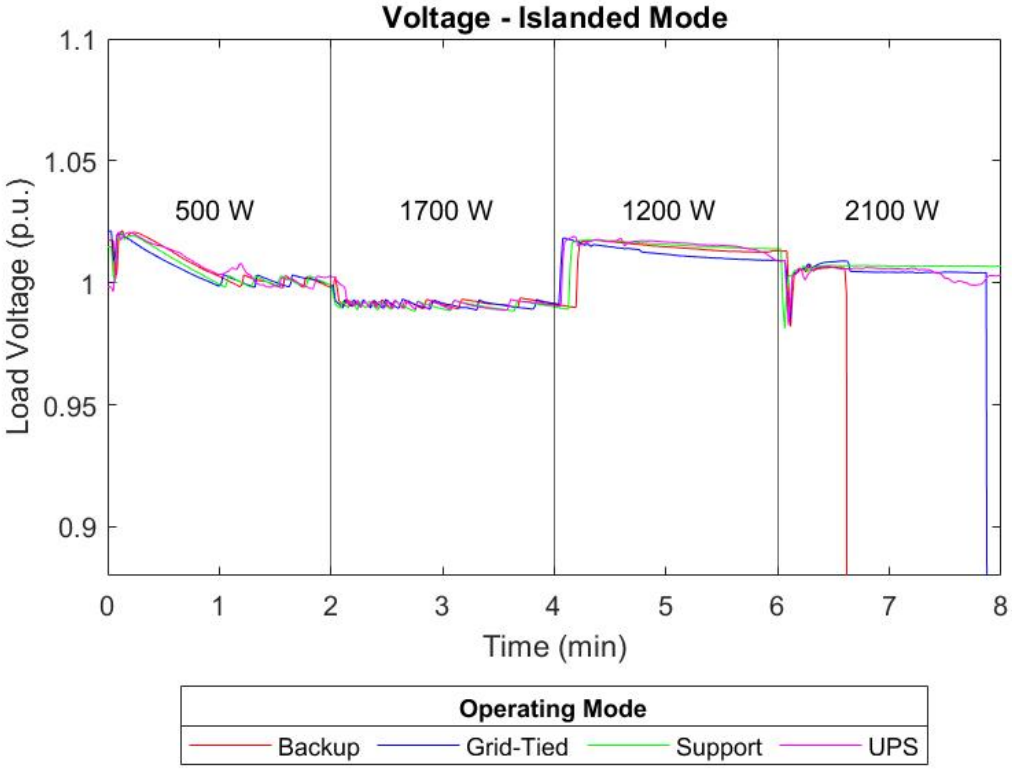

Figure 4.4. The load voltage profiles of each operating mode for a given step-load test in islanded mode.

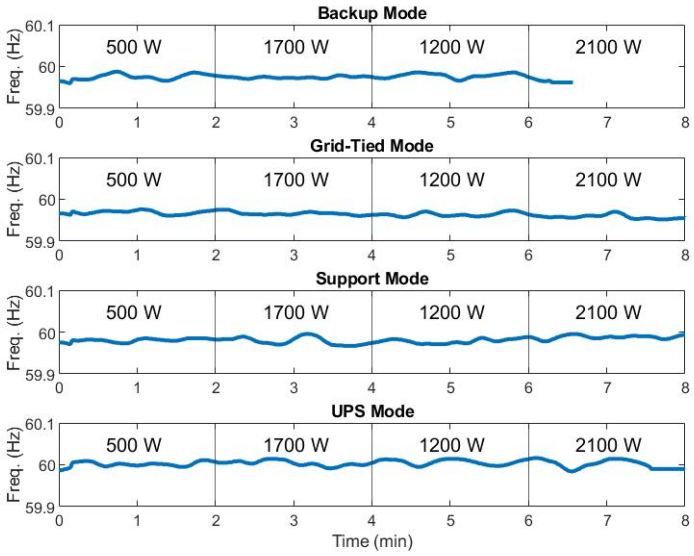

Figure 4.5. Load voltage frequency profiles of each operating mode for a given step-load test in grid-connected mode.

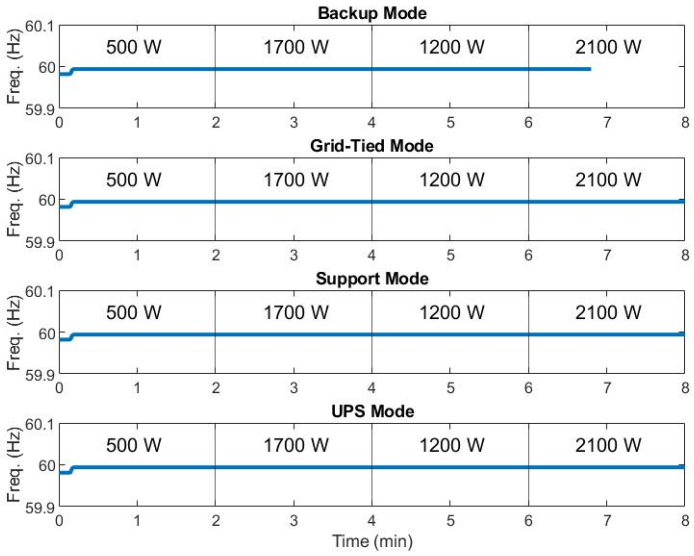

Figure 4.6. Load voltage frequency profiles of each operating mode for a given step-load test in islanded mode.

IEEE Standard 1547 requires that an active DER in the continuous operation region have a voltage of 0.88 p.u. to 1.10 p.u. The load voltage in both a grid-connected state and an islanded state, for this microgrid, show compliance with the standard in this regard. It is noteworthy to observe that the voltages for each operating mode, when in a grid-connected AC input state, are less than the nominal (120 V). However, when in an islanded state, the load voltages remain approximately at the nominal. The deduction is that when the microgrid is operating in an islanded state, it more efficiently routes the power from the batteries through the inverter and to the load, as opposed to when it receives and routes power from the local EPS. Additionally, when the microgrid is operating in islanded state, the system operation mode appears to have little effect on the output, as the voltage profiles are quite similar. However, the distortion (although small) in the voltage waveforms is apparent and should be taken into consideration.

Another observation of this test is that the frequency of the system output load remains relatively unchanged throughout any step in the load, for both grid-connected and islanded AC input states. In fact, when in an islanded state, the microgrid remained at 60 Hz in every system operating mode but had some degree of variation in the grid-connected state. This, again, leads to the deduction that the system is more effective when it creates its own power from the external DC power source than when it is connected to an outside AC input source.

4.2.2 AC Input Switching Test

The second test began with a 1200 W load in a grid-connected mode and switched to islanded mode, back to grid-connected mode and then again to islanded mode. This repetition allowed for a better understanding of the switching response of the microgrid. Each phase of the trials was two minutes in length, allowing the microgrid to reach a steady-state condition. Table 4.2 provides a list of the experiments conducted for this test. The load voltage profiles are shown individually while the load frequency profiles are included in one figure.

Table 4.2. Experimental Trials for AC Switching for Voltage and Frequency Ride-Through

Experiment#	Operating Mode	Voltage/Frequency	Figure
1	Backup	Voltage	Figure 4.7
2	Grid-Tied	Voltage	Figure 4.8
3	Support	Voltage	Figure 4.9
4	UPS	Voltage	Figure 4.10
5	All Modes	Frequency	Figure 4.11

When the system is in an islanded operating state for the grid-tied operating mode (Figure 4.8) and is given the command to switch back to a grid-connected state (via the control system interface), the delay time to enact that command is approximately three minutes, as opposed to a nearly instant switching time for the microgrid when in the other three operating modes. Figures 4.7, 4.9 and 4.10 show that there is a consistent difference in the output voltage of the microgrid when operating in a grid-connected operating state versus an islanded state. In both operating states, some voltage oscillations are visible but not significant such that the voltage is ever outside of the overvoltage/undervoltage window set in IEEE Standard 1547-2018. Additionally, Figure 4.11 shows that the frequency, while in any operating mode, remains consistently within the range specified in the IEEE standard.

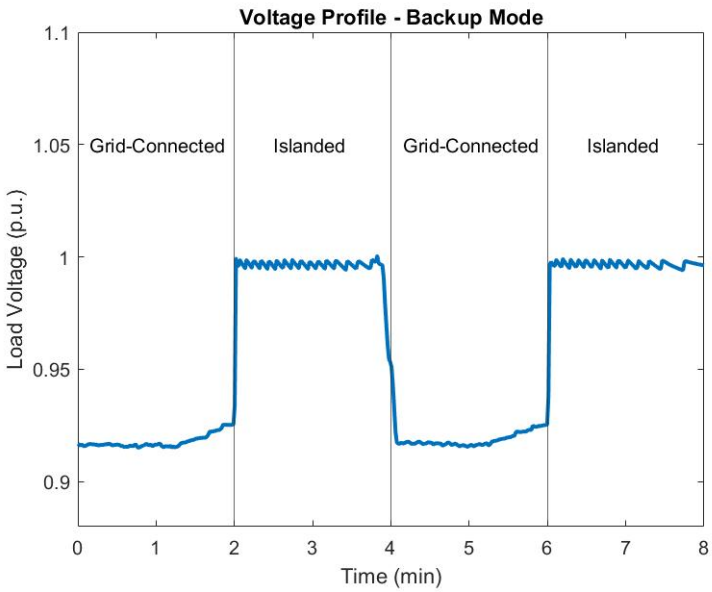

Figure 4.7. Load voltage (p.u.) during Experiment 1 in backup mode

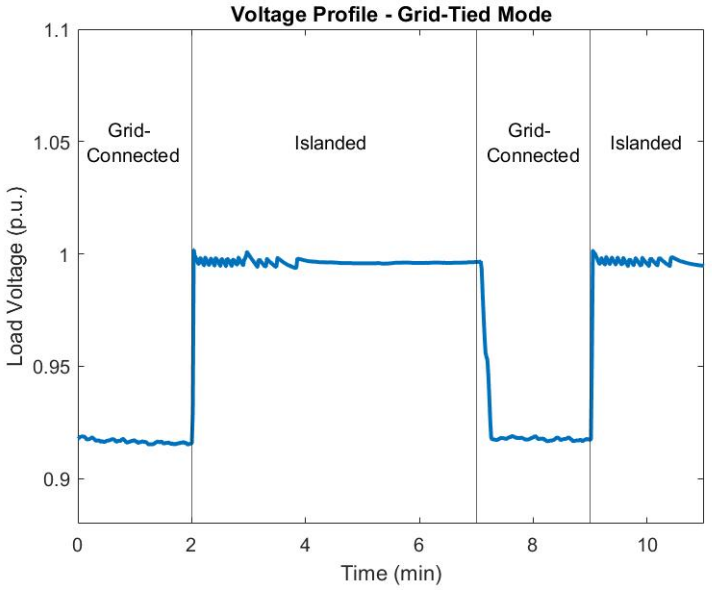

Figure 4.8. Load voltage (p.u.) during Experiment 2 in grid-tied mode

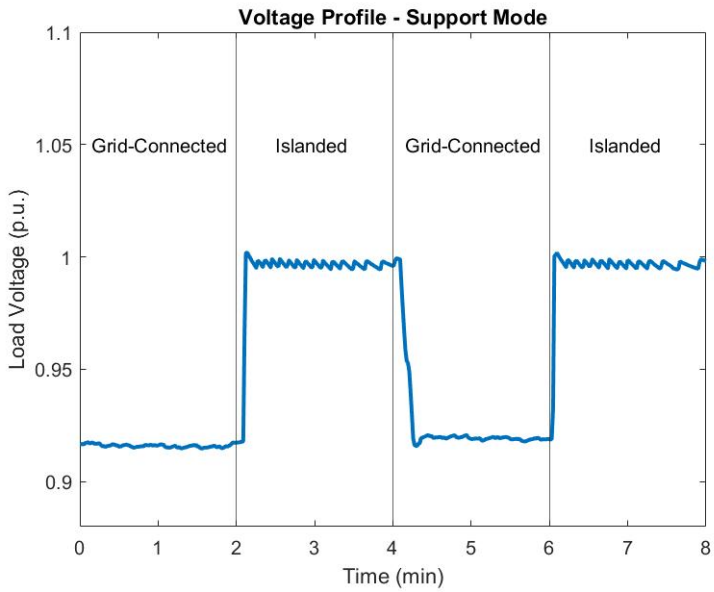

Figure 4.9. Load voltage (p.u.) during Experiment 3 in support mode

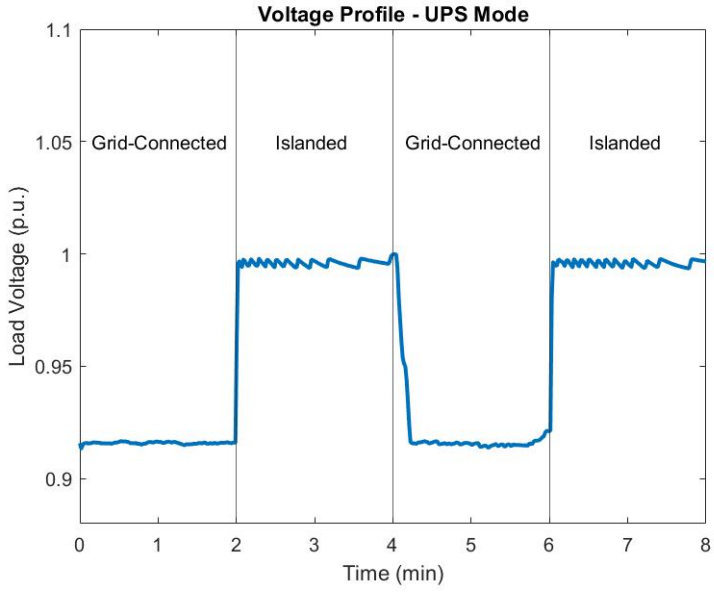

Figure 4.10. Load voltage (p.u.) during Experiment 4 in UPS mode

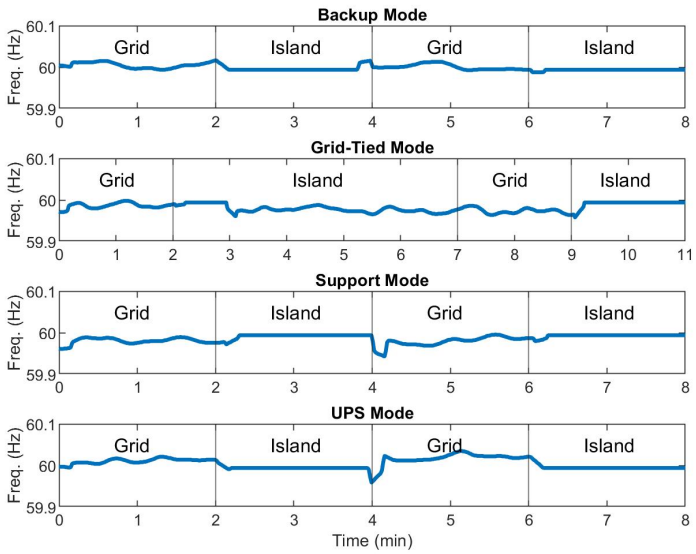

Figure 4.11. Experiment 5: The microgrid is in a grid-connected state for the phases labeled, "grid," and is in an islanded state for the phases labeled, "island."

Similar to the results of the step-load test on the microgrid, changing between AC input sources does not show any overvoltage/undervoltage or overfrequency/underfrequency values that place the system outside of the continuous operation range, for any of the tested operating modes. A steady-state operating condition is never fully reached at two minutes when in an islanded state, indicating that the system voltage continues to oscillate after that time period. These oscillations are small, though, and would not likely have great effect on a load, as they did not have an effect on the load operation during the execution of these experiments. Aside from the time lag for the grid-tied operating mode, there is no discernible difference between the functionality of any of the four operating modes for either the voltage or the frequency.

4.3 Transient Response and AC Switching

The Fluke 434 has the ability to monitor voltages and currents for several hours or days on the Voltage/Amps/Hertz display setting at a rate of five readings per second but can

provide, at a minimum, a one-second resolution for output data [26]. As such, the voltage levels obtained in Section 4.2 provide information to assess the operational capabilities of the microgrid for different load values and AC source inputs, but they do not fully capture the transient, or the moment of transition between operational states.

The transient response of the system is an important aspect to characterize because of its capacity to sustain power to a load. In the event of an intentional or unintentional grid-connection failure, the inverter must transition the power supply from the AC source (the local EPS or the generator) to the DC power supply (through the power converter). This transition, though often less than one second, is not always instantaneous, and for certain loads, the delay between the power supply failure and activation could fault the load system, causing it to shut down or fail.

To evaluate this operational capability of the microgrid, a test was conducted using the oscilloscope (from Section 3.8) to capture the transient response of the microgrid for the four operating modes when transitioning from a grid-connected state to an islanded state. This simulates a grid-connection failure. To contrast this instrument with the Fluke 434, the oscilloscope is capable of providing a resolution of 60.6 pico-seconds, enabling this measurement instrument to appropriately observe the transient response of the system when transitioning between AC input sources. While monitoring the waveforms of the load voltage, load current and local EPS current, the trigger of the oscilloscope was set to capture the moment that the local EPS failed and went to zero. Table 4.3 displays the list of experiments conducted for this test and the corresponding figures where all three waveforms are provided in addition to a single view of the load voltage, for evaluation of compliance to IEEE Standard 1547.

Table 4.3. Experimental Trials for Microgrid Transient Response

Experiment#	Operating Mode	Waveforms	Figure
1	Backup	All	Figure 4.12
1	Backup	Voltage	Figure 4.13
2	Grid-Tied	All	Figure 4.14
2	Grid-Tied	Voltage	Figure 4.15
3	Support	All	Figure 4.16
3	Support	Voltage	Figure 4.17
4	UPS	All	Figure 4.18
4	UPS	Voltage	Figure 4.19

Figure 4.12 shows that there is a defined break in the load voltage and current when exposed to grid failure. The transient time between grid failure and voltage stabilization is measured in Figure 4.13 to be 9.1 ms, though there is clear but minimal distortion of the voltage following stabilization that was not present prior to the failure.

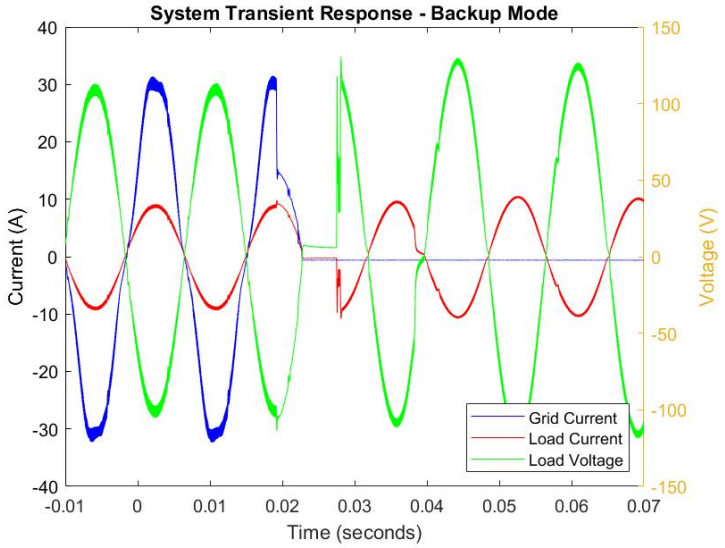

Figure 4.12. Oscilloscope waveforms during Experiment 1 in backup mode

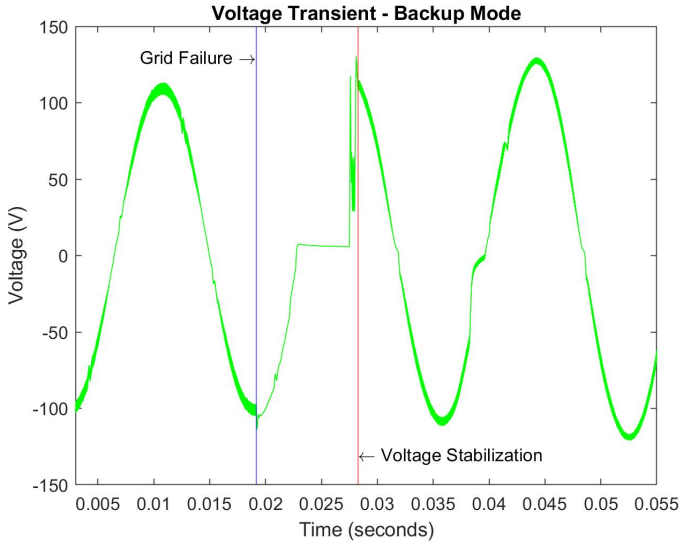

Figure 4.13. Load voltage during Experiment 1 in backup mode

There is also a clear disruption in the load voltage and current when exposed to grid failure in grid-tied mode, as shown in Figure 4.14. The transient response of the voltage was measured from Figure 4.15 to be 9.3 ms, and similar to the results of Experiment 2, there is clear distortion in the voltage signal after it stabilizes.

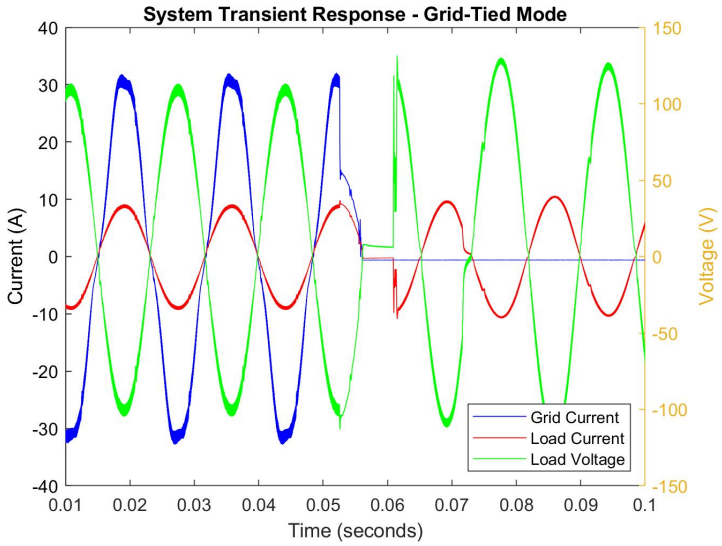

Figure 4.14. Oscilloscope waveforms during Experiment 2 in grid-tied mode

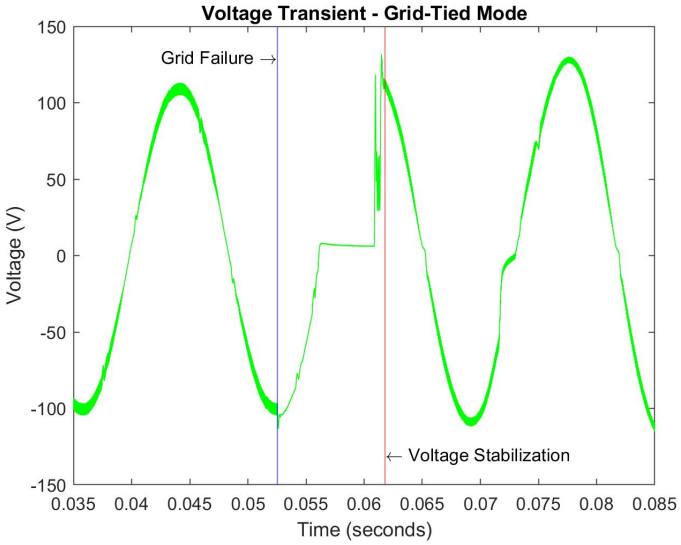

Figure 4.15. Load voltage during Experiment 2 in grid-tied mode

Similar to Experiments 1 and 2, the voltage and current profiles in Figure 4.16 for Experiment 3 show that the voltage and current go to zero at the time of grid failure when in support mode. The transient time for the stabilization of those waveforms is 9.2 ms, and the distortion shown in Figure 4.17 is nearly the same as the results of Experiments 1 and 2.

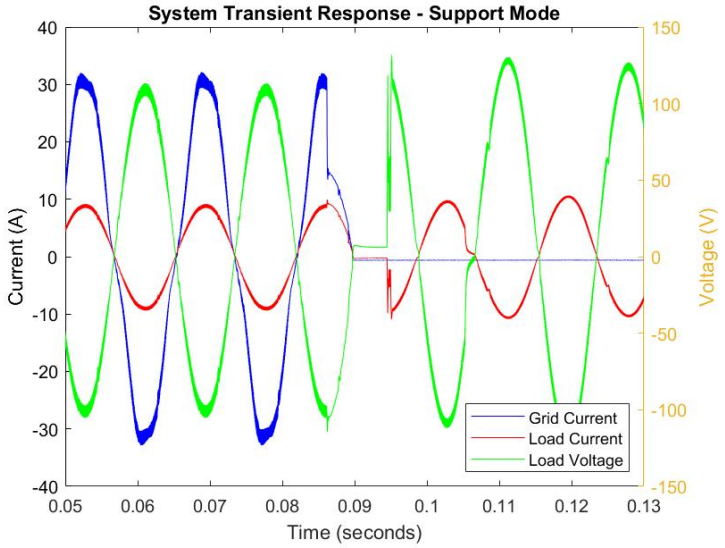

Figure 4.16. Oscilloscope waveforms during Experiment 3 in support mode

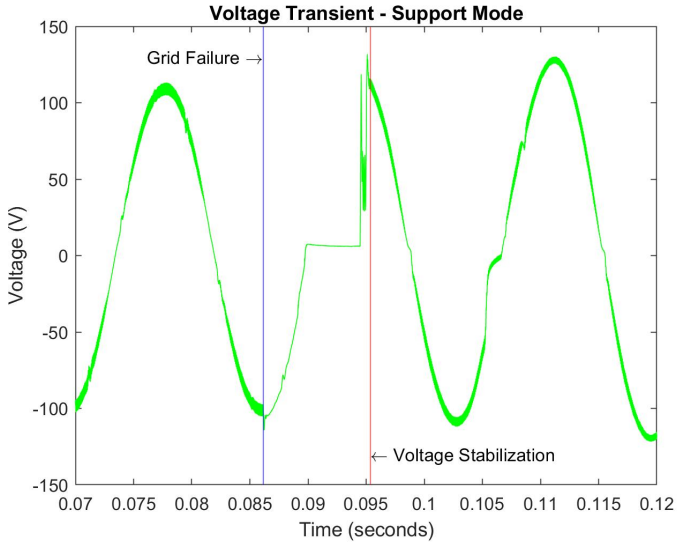

Figure 4.17. Load voltage during Experiment 3 in support mode

When exposed to grid failure while in UPS operating mode, the load voltage and current, shown in Figure 4.18, do not show any true sign of breaking. There is no zeroing that occurs, and stabilization of the load voltage, shown in Figure 4.19, occurs in 1.9 ms, with little to no distortion present afterward.

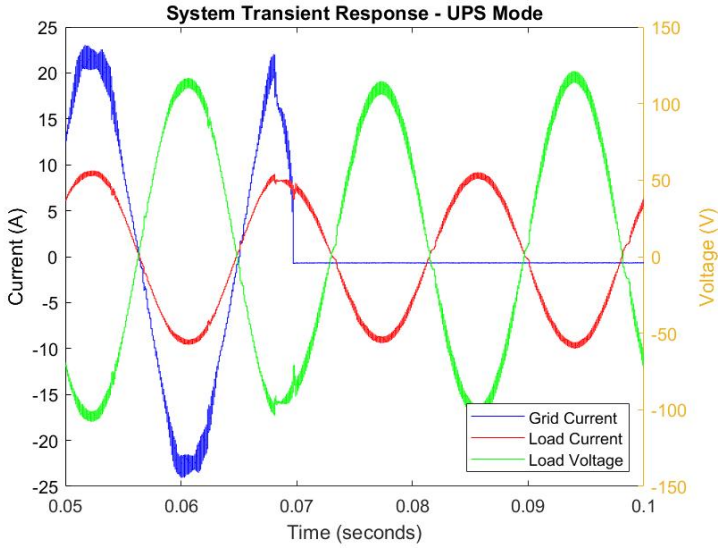

Figure 4.18. Oscilloscope waveforms during Experiment 4 in UPS mode

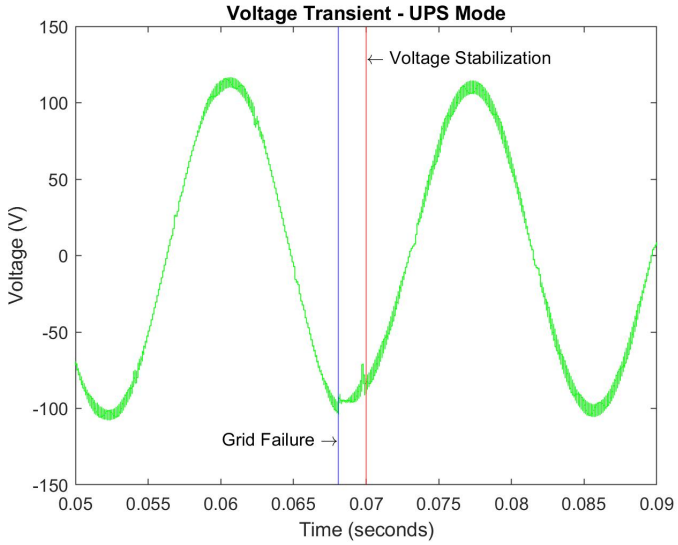

Figure 4.19. Load voltage during Experiment 4 in UPS mode

IEEE Standard 1547, Clause 6.4.2.2, provides a relaxation to the voltage ride-through regulation that allows temporary deviations of power for up to 0.5 s that cause the DER voltage to go outside of the acceptable levels [4]. As zero voltage is outside of that acceptable level, any system transient response must be less than that accepted relaxation time. Observation of the transient responses in Figures 4.12 - 4.19 show that no operating mode is in violation of Clause 6.4.2.2. It is also noted that within the Outback Power manual, the UPS operating mode is said to have the fastest switching response time [22], and this is evident, as the UPS transient response from grid failure to a stabilized voltage is approximately five times faster than that of the backup operating mode. While all of the operating modes provide a fast transient response (relative to the standard) when exposed to grid failure, the UPS mode does, in fact, provide the best response, which is critical when providing power to sensitive loads.

4.4 Harmonic Distortion

The standard fundamental frequency of a local EPS in the U.S. is 60 Hz. An ideal voltage or current sine wave will oscillate at this frequency alone, resulting in a pure signal, but because of natural frequency variations within a system, resulting from the presence of non-linear devices [27], these ideal signals do not occur. As such, harmonic distortion, or variation in the frequency which results in a non-ideal or distorted signal, exists in a system. The greater the amount of distortion in the signal, the greater the chance is to cause a disturbance that could result in damage to the system. Figure 2.3 provides the IEEE Standard 1547-2018 total acceptable current harmonic distortion at the point of connection between a DER and the local EPS.

A test was conducted to measure the total harmonic distortion of this COTS microgrid in accordance with the standard. The microgrid was loaded with a 1200 W load in every experimental trial for testing consistency, and the steady-state harmonic distortion for both the load voltage and current was measured in both grid-connected and islanded operating states, for five minutes in each state. IEEE Standard 1547-2018 does not contain limitations on voltage distortion, due to an expectation of the presence of background voltage distortion from the EPS [4]. However, observation of the voltage distortion for a COTS microgrid is an important aspect to consider for potentially sensitive loads, so it is included in this thesis.

Table 4.4 provides the list of experimental trials conducted for this test and the corresponding figures with the waveforms each displayed for the four practical operating modes. The measurement instrument used for this test was the Fluke 434, which only provides the harmonic distortion measurements for the three most dominant non-fundamental odd harmonics: the third, fifth and seventh. The total distortion for each experiment is the summation of these three harmonics. The Fluke 434 is able to measure the voltage and current harmonic distortion simultaneously, so there were a total of four experiments conducted, as noted in the table.

Table 4.4. Experimental Trials for Voltage and Current Harmonic Distortion

Experiment#	Operating Mode	Voltage/Current	Figure
1	Backup	Voltage	Figure 4.20
1	Backup	Current	Figure 4.21
2	Grid-Tied	Voltage	Figure 4.22
2	Grid-Tied	Current	Figure 4.23
3	Support	Voltage	Figure 4.24
3	Support	Current	Figure 4.25
4	UPS	Voltage	Figure 4.26
4	UPS	Current	Figure 4.27

The distortion measured in Figures 4.20 and 4.21 remain reasonably consistent throughout the experiment, with a notable spike at the transition moment between AC input sources. Distortion is higher when in an islanded operating state, and compared to the voltage, the current distortion is also higher.

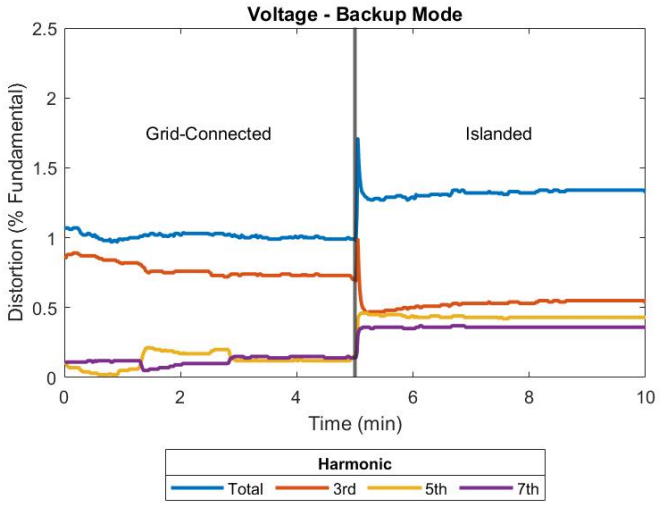

Figure 4.20. Experiment 1 - Voltage harmonics

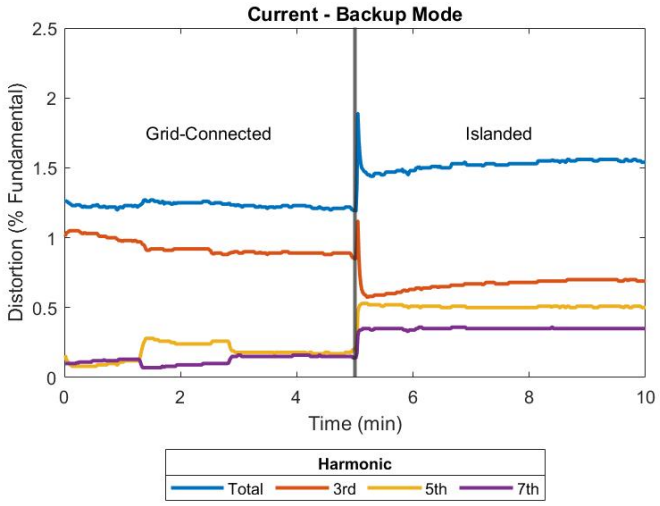

Figure 4.21. Experiment 1 - Current harmonics

Figures 4.22 and 4.23 show a decrease in the voltage and current distortions while grid-connected, which can reasonably be explained by a stabilization of the connection between the microgrid and the EPS. The distortions in grid-tied mode when in an islanded operating state remain consistent throughout the experimental duration.

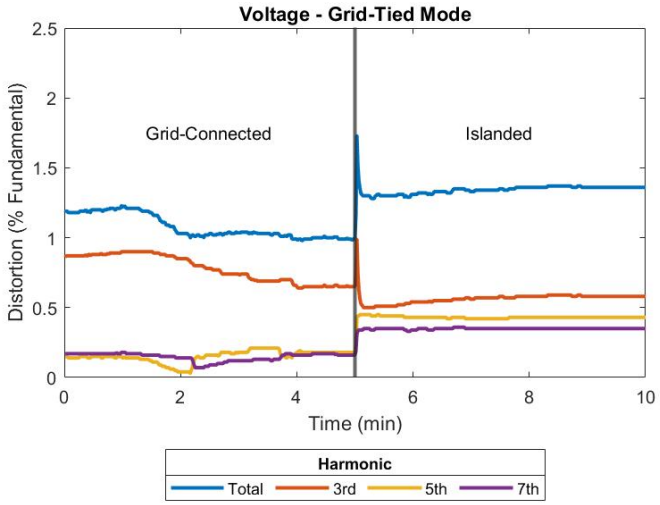

Figure 4.22. Experiment 2 - Voltage harmonics

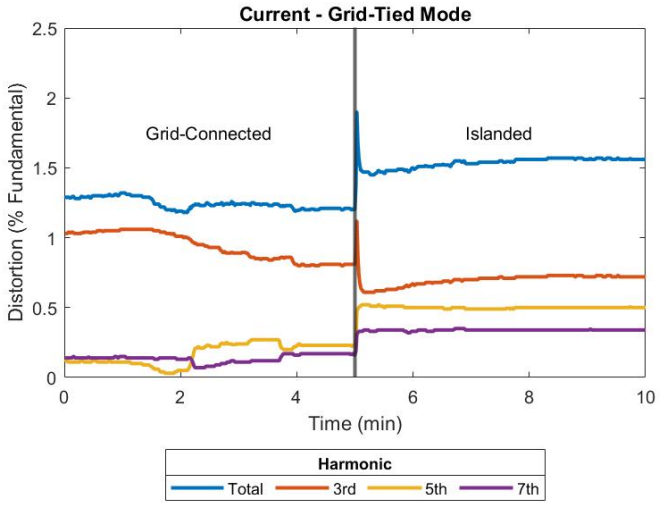

Figure 4.23. Experiment 2 - Current harmonics

The voltage and current distortions while in support operating mode, shown in Figures 4.24 and 4.25, are at a lower value than either backup or grid-tied operating modes when in a grid-connected state. This is because the microgrid is disconnected from the EPS when in support mode, whereas it remains connected during backup and grid-tied modes.

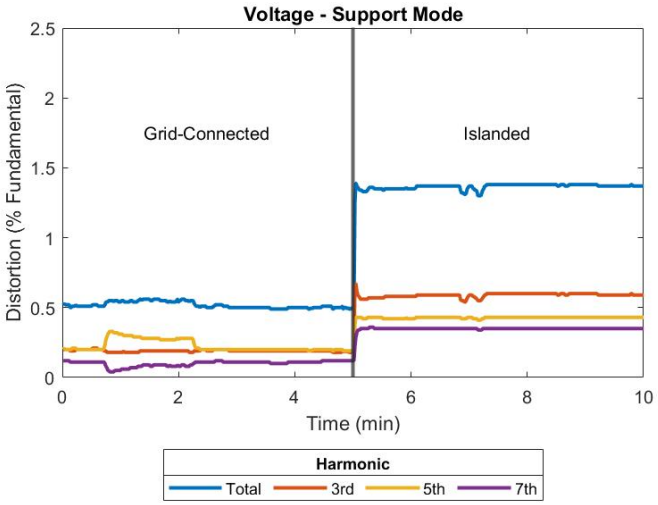

Figure 4.24. Experiment 3 - Voltage harmonics

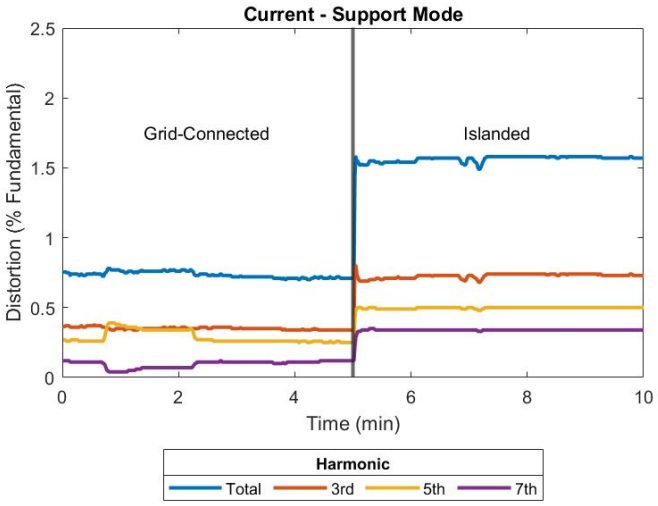

Figure 4.25. Experiment 3 - Current harmonics

Similar to grid-tied mode, when the microgrid is in UPS mode, it is constantly monitoring the connection to the EPS, so the distortion decrease shown in Figures 4.26 and 4.27 can be explained as a stabilization period between the microgrid and the EPS.

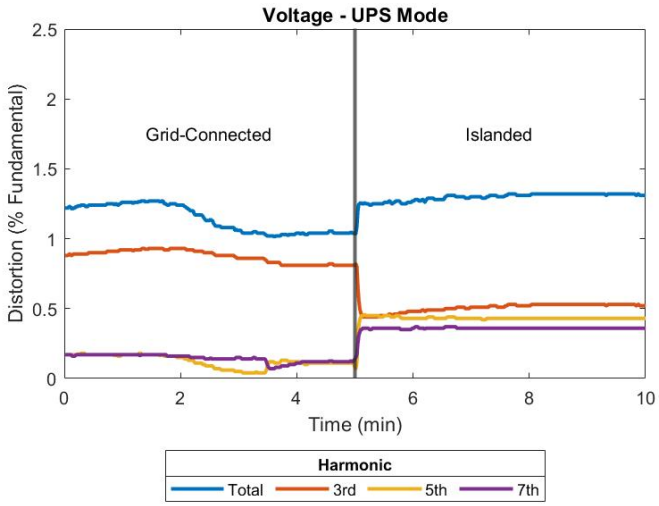

Figure 4.26. Experiment 4 - Voltage harmonics

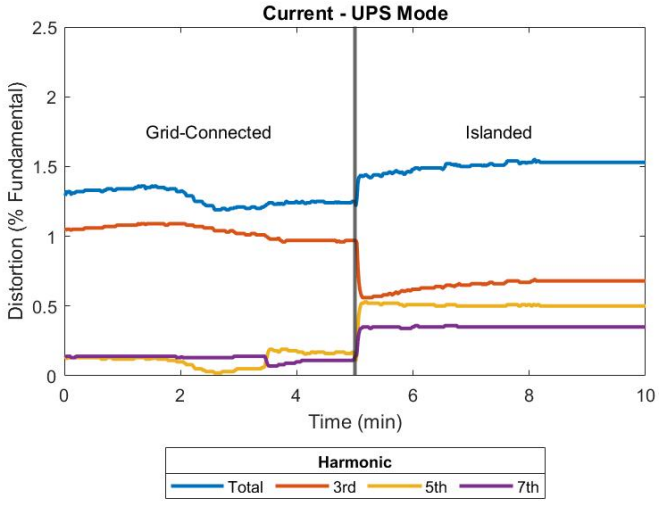

Figure 4.27. Experiment 4 - Current harmonics

The total rated-current distortion (TRD) maximum limit provided in IEEE Standard 1547-2018 is 5% of the rated current[1]. In every experimental trial, the microgrid was compliant to the standard, with TRD consistently under 2% of the rated current. Additionally, it can be observed that the distortion, for both voltage and current, had a higher but more consistent value in an islanded operating state than in a grid-connected state. When in a grid-connected state, the system adjusts to the frequency of the local EPS which has natural distortion, but in an islanded state, the system operates independently of the EPS and is able to better maintain a consistent frequency. The distortion present in the system during an islanded operating state is due primarily to the internal system components and their non-linearity.

4.5 Balance of Power

An ideal system would yield a 100% efficiency, and all of the power that goes into the system would be used by the system with no power losses. Because most systems are subject to losses that result from power conversions, component degradation and other factors, a 100% efficient system is unrealistic. However, it is almost always a goal to design a system to be as efficient as possible by minimizing the losses. This, in turn, minimizes the amount of input power consumed by the system and makes the system more environmentally and economically friendly.

Equation 4.1 displays the simple relation of the balance of power for this COTS microgrid.

$$Power_{in} = Power_{out} + Power_{losses} \tag{4.1}$$

The total input power for this microgrid system is the summation of the DC power generated by the PV array, the battery power discharged into the power converter and the AC power consumed from the local EPS. These three inputs are not always active at the same time, though. For example, when the microgrid is in an islanded operating state, the input power comes from the PV array and the batteries but not from the EPS. It is possible to have the input power consist of all three of these inputs simultaneously, if the load demand is high

[1]The standard defines only the current distortion range and specifies it as "total rated current distortion" [4], but the voltage harmonic distortion is included in this thesis because of its relative importance when discussing sensitive loads.

enough that the AC input source cannot supply adequate power. For a load demand that is able to be supplied by the AC source, though, the input power then becomes a summation of two sources: either the AC source and the PV array or the battery discharge power and the PV array.

The assumed output power for this microgrid is the summation of the loads and the battery recharge power. When the microgrid is in a grid-connected state, the batteries are in a charging mode and draw power from both the AC source and from the PV array (depending on the power inverter operating mode). The only exception is when the load demand is too great for the AC source to supply, at which point the batteries are then considered an input power source. The difference between the input power and the output power can be considered the system loss power and is the characteristic to be observed.

A test was conducted on this COTS microgrid to determine the average power loss. The microgrid operated for a 24-hour period of time, similar to the test conducted in Section 4.1. The system sustained a consistent load during each of the experiments (700 W, 1200 W and 2100 W), and the average power loss and system efficiency were calculated after each experiment. The data for this test was generated using OpticsRE, the online data-collection platform from Outback Power. This data was generated in 15-minute intervals over the 24-hour period, and Table 4.5 displays the details of each experiment.

Table 4.5. Experimental Trials for Balance of Power

Experiment#	Load (W)	Avg. Power Loss (W)	Efficiency (%)	Figure
1	700	33.2	90	Figure 4.28
2	1200	29.5	94	Figure 4.29
3	2100	19.4	96	Figure 4.30

The microgrid spends a majority of the 24-hour duration in Figure 4.28 in an islanded operating state (61% of the duration), indicating that the power generated by the PV array is more capable of supporting the battery-charging capacity than in the other trials. By contrast, the microgrid operated in the islanded operating state for 43% of the time in Figure 4.29 and 16% of the time in Figure 4.30.

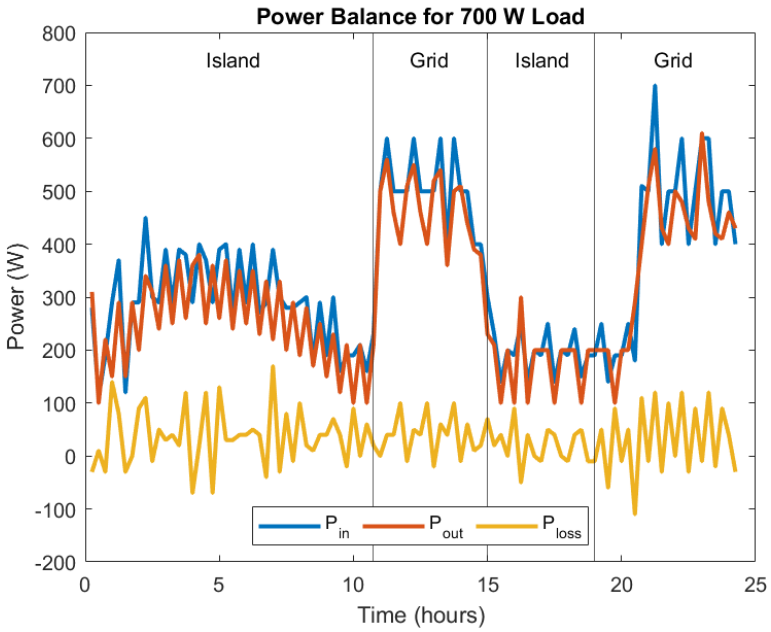

Figure 4.28. Experiment 1 - 700 W

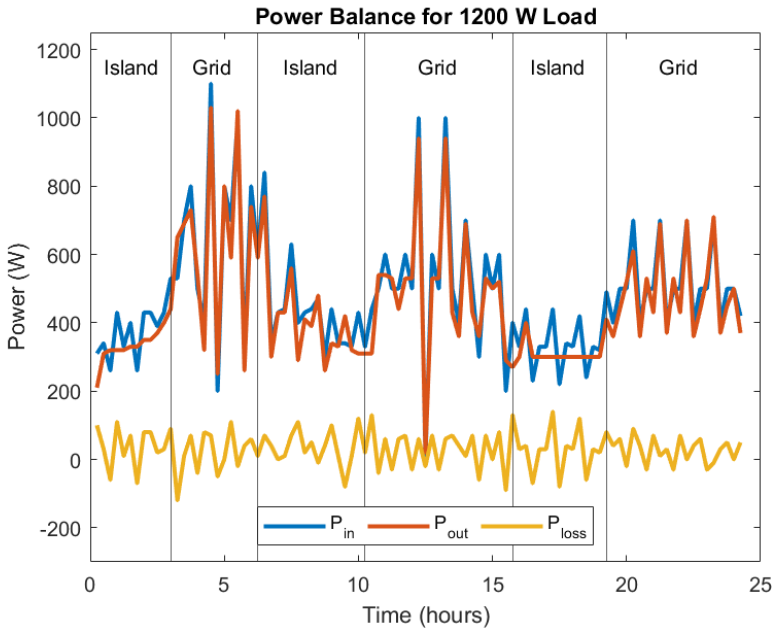

Figure 4.29. Experiment 2 - 1200 W

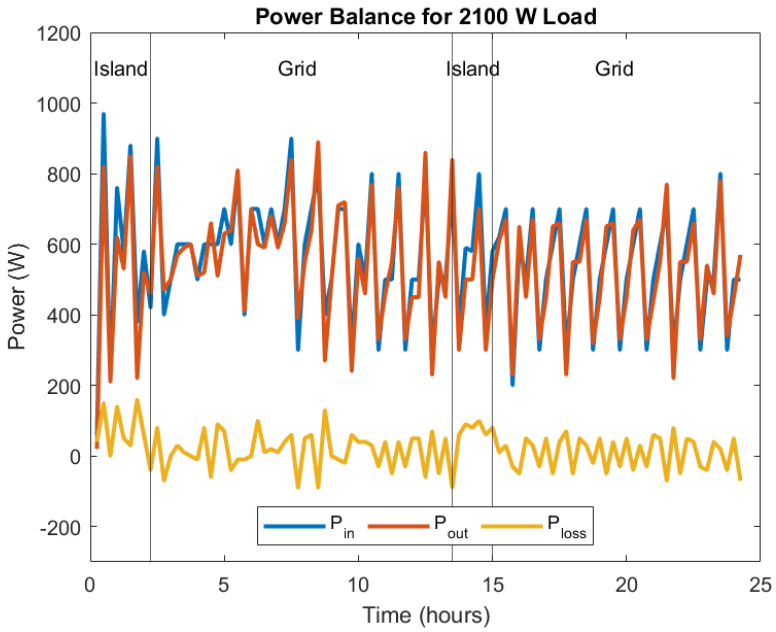

Figure 4.30. Experiment 3 - 2100 W

The observable variation in the power levels for the microgrid is due to three main effects: the inconsistency of the solar irradiation on the PV panels, generating DC power for the batteries, the variation in the load demand, as the inductive motor changes depending on the immediate atmosphere external to the heater, and the SOC variation, as a result of the solar irradiation and the current going into and out of the batteries. Additionally, because OpticsRE only provides data at 15-minute intervals, any smoothness to the collected data is difficult to obtain. However, despite the variable nature of the input, output and loss power profiles, there are observable trends. The lightest load yielded the highest power loss (33.2 W) and the worst overall efficiency (90%) of the three experiments. Efficiency was calculated using Equation 4.2.

$$Efficiency = (Power_{in,average} - Power_{out,average})/(Power_{in,average}) \tag{4.2}$$

The power generated by the microgrid is greater when connected to the local EPS which is understandable, as the input power produced by the AC source is offset by the recharging power consumed by the batteries. The microgrid also operates at a greater efficiency for a higher load demand, which is typical in power electronic systems. The average efficiency rating for this COTS microgrid is 92%, per the specification sheet in [22].

4.6 Summary

This chapter has illustrated the operational characteristics of this COTS microgrid. Individual examination of each of these characteristics clarifies how this microgrid will operate for a certain load demand. This information can be used for the purposes of military operations for known information about the loads that will be connected to the microgrid. For example, if a sensitive load cannot sustain even a small duration of zero-voltage during a grid failure, then that load must operate only under the UPS operating mode. Understanding the capabilities and limitations of the microgrid provides critical information to leaders when making operational decisions.

CHAPTER 5:
Conclusions and Future Work

5.1 Conclusions

This thesis provides insight into the functionality of a COTS mobile microgrid and compares its performance against the voltage and current specifications in IEEE Standard 1547-2018. In addition to the characteristics that are directly comparable to the standard, other factors were tested and observed to determine whether or not this COTS system might adequately serve sensitive loads for military operations. Table 5.1 displays each of the microgrid characteristics tested and analyzed in this thesis, their applicable compliance to the IEEE standard and notes about the test results.

Table 5.1. List of microgrid characteristics tested and analyzed in this thesis

Characteristic	**IEEE Compliant**	**Notes**
Battery Charge	N/A	700 W Trial: 66% time spent islanded 1400 W Trial: 42% time spent islanded 2100 W Trial: 13% time spent islanded
Ride-Through	Yes	Grid-Connected load voltage: 110 V Islanded load voltage: 120 V Frequency in islanded state very stable
Transients	Yes	Longest transient time = 9.3 ms UPS transient time = 1.9 ms
Power Quality	Yes	Voltage and current distortion under 2%
Power Balance	N/A	700 W Trial: 33.2 W lost, 90% efficient 1200 W Trial: 29.5 W lost, 94% efficient 2100 W Trial: 19.4 W lost, 96% efficient

From the experimental trials and data presented in this thesis, it can be concluded that the COTS microgrid analyzed can adequately support varying load demands. In an islanded operating state, the microgrid has the ability to support smaller loads for multiple hours while supplying a consistent voltage and frequency level to the output. As expected, greater loads in an islanded state result in a diminished sustainable operating time. In a grid-connected state, the microgrid is capable of maintaining standard-compliant voltage and frequency at the PoC such that there is little to no risk of disrupting the voltage and frequency continuity of the EPS. Grid-connected operation can be indefinite when a utility grid is available, given that the point of interconnection remains within the IEEE standard.

The microgrid also has the ability to switch between a grid-connected and an islanded state without disrupting the power flow to the loads, with the UPS operating mode providing the best transient response. This operating mode is highly recommended for sensitive loads. For three 24-hour trials at different load demands, the microgrid performed with a 90% or greater efficiency level and minimized the power losses. In total, this COTS microgrid was compliant to IEEE Standard 1547-2018, when applicable, and displayed an ability to efficiently provide power to the loads.

The results of this thesis can be used as a template to characterize other COTS microgrids. Utilizing the format of Table 5.1 and the tests conducted in Chapter 4, these characteristics can be experimentally determined for many different microgrids. This work would provide the ability to determine trends for many COTS microgrids and also to create a best-fit solution to a given operational scenario.

5.2 Future Work

This thesis analyzed the compliance of specific characteristics of this COTS microgrid to IEEE Standard 1547-2018, but there are many other COTS components and systems available. While the results of this work show that this particular system provides consistent and efficient power to the loads, other COTS systems may be considered in support of different military operations, whether in facilities or in forward operating bases. As such, an option for future work is to accurately model this microgrid using computer software and then to simulate other COTS components and systems, providing analysis for various system setups and the loads that they are best able to service. Additional work with this concept

could include sensitive loads and how they are able to operate with COTS components, to determine their feasibility in support of various military operations.

Another option for future work with COTS microgrids is in protection against cyber attacks. The COTS microgrid used in this thesis connects to the internet through the OpticsRE interface, and other COTS systems have similar connections. Research into the security of these system interfaces and how to best protect them from cyber attacks would produce helpful results, especially if these systems can be used for military operations. Continued analysis of COTS microgrids could have a significant impact on the energy consumption and environmental sustainability of military facilities and mobile installations.

THIS PAGE INTENTIONALLY LEFT BLANK

List of References

[1] M. Lamonica, "Hybrid Generator Would Cut Military Base Fuel Costs in Half," IEEE Spectrum, Feb. 3, 2014 [Online]. Available: https://spectrum.ieee.org/hybrid-generator-would-cut-military-base-fuel-costs-in-half

[2] B. Capehart, "Distributed Energy Resources," WBDG, Oct. 10, 2016 [Online]. Available: https://www.wbdg.org/resources/distributed-energy-resources-der

[3] Office of the Federal Chief Sustainability Officer - Council on Environmental Quality, *Federal Agency Progress Data and OMB Scorecard*, 2022 [Online]. Available: https://www.sustainability.gov/dod.html#btu

[4] *IEEE Standard for Interconnection and Interoperability of Distributed Energy Resources with Associated Electric Power Systems Interfaces*, IEEE Standard 1547-2018, 2018.

[5] H. Lu, G. Wu, and H. Biyawerwala, "Application of IEEE 1547-2018 on Large-scale DER Interconnections with Proposed Operation Mode and Control Method," in *2020 IEEE/PES Transmission and Distribution Conference and Exposition*, 2020 [Online]. Available: https://ieeexplore.ieee.org/stamp/stamp.jsp?tp=&arnumber=9300006

[6] R. Mahmud, A. Hoke, and D. Narang, "Fault Response of Distributed Energy Resources Considering the Requirements of IEEE 1547-2018," in *2020 IEEE Power and Energy Society General Meeting*, 2020 [Online]. Available: https://www.nrel.gov/docs/fy20osti/75046.pdf

[7] M. Vygoder, G. Oriti, J. Gudex, T. Tencate, A. Julian, and R. Cuzner, "Comparison of Voltage Abnormality Detection Methods for Single-Phase Inverters to Meet the Requirements in IEEE Standard 1547-2018," *IEEE Transactions on Industry Applications*, vol. 57, no. 5, Sep. 2021 [Online]. doi: https://ieeexplore.ieee.org/stamp/stamp.jsp?tp=&arnumber=9445655.

[8] T. Tencate, G. Oriti, and A. Julian, "Comparison of Control Methods for Single-Phase Inverters to Meet the Requirements in IEEE Standard 1547-2018," in *2020 IEEE International Conference on Environment and Electrical Engineering*, 2020 [Online]. Available: https://calhoun.nps.edu/bitstream/handle/10945/65809/Oriti_Comparison_of_Control_Methods.pdf?sequence=1&isAllowed=y

[9] N. Ninad, E. Apablaza-Arancibia, M. Bui, and J. Johnson, "Commercial PV Inverter IEEE 1547.1 Ride-Through Assessments Using an Automated

PHIL Test Platform," *Energies*, vol. 14, no. 6936, Oct. 2021 [Online]. doi: https://www.proquest.com/docview/2596026209/fulltextPDF.

[10] A. Lantero, "How Microgrids Work," Department of Energy, Jun. 17, 2014 [Online]. Available: https://www.energy.gov/articles/how-microgrids-work

[11] X. Yan, W. Yu, Z. Cuo, and L. Zhengmao, *Coordination of Distributed Energy Resources in Microgrids*, 1st ed. London, United Kingdom: The Institution of Engineering and Technology, 2021.

[12] S. Padmanaban and K. Nithiyananthan, *Microgrids*, 1st ed. Boca Raton, FL, USA: CRC Press, 2021.

[13] D. Xinzhou and S. Shenxing, *Fault Location and Service Restoration for Electrical Distribution Systems*, 1st ed. Solaris South Tower, Singapore: John Wiley and Sons Singapore Pte. Ltd., 2016.

[14] *American National Standard for Electric Power Systems and Equipment - Voltage Ratings (60 Hertz)*, ANSI Standard C84.1, 2020.

[15] B. Rausch, "What Texans Need to Know About ERCOT's Power Warnings and Possibility of Rolling Blackouts," Houston Chronicle, Jul. 11, 2022 [Online]. Available: https://www.houstonchronicle.com/business/energy/article/What-Texans-need-to-know-about-ERCOT-s-power-17297277.php

[16] "Honeywell 1,500W Ceramic Electric Space Heater," August 28, 2022 [Online]. Available: https://www.menards.com/main/heating-cooling/heaters/space-heaters/honeywell-1-500w-ceramic-electric-space-heater/hhf360v.htm

[17] "Government Employee Computer Pictures, Images and Stock Photos," August 28, 2022 [Online]. Available: https://www.istockphoto.com/photos/government-employee-computer

[18] Office of Energy Efficiency and Renewable Energy, "Solar Radiation Basics," Accessed Jul. 20, 2022 [Online]. Available: https://www.energy.gov/eere/solar/solar-radiation-basics

[19] Outback Power, *FLEXmax Series Charge Controllers Owner's Manual*, 2020 [Online]. Available: https://www.outbackpower.com/downloads/documents/charge_controllers/flexmax_6080/owner_manual.pdf

[20] GS Yuasa Energy Solutions, *Technical Overview of the SLR Super Long Cycle Life Family of Valve Regulated, Lead Acid Batteries*, 2019 [Online]. Available: https://gsyuasa-es.com/Downloads/SLR_Tech_Overview.pdf

[21] C. Woodford, “Battery chargers,” Explain That Stuff, Apr. 25, 2021 [Online]. Available: https://www.explainthatstuff.com/how-battery-chargers-work.html

[22] Outback Power, *FXR Series Inverter/Charger Operator’s Manual*, 2017 [Online]. Available: https://www.outbackpower.com/downloads/documents/inverter_chargers/fxr_vfxr_a/fxr_operator.pdf

[23] N. Mohan, T. Undeland, and W. Robbins, *Power Electronics: Converters, Applications and Designs*, 2nd ed. Chichester, West Sussex, United Kingdom: John Wiley and Sons, 1995.

[24] Q.Zhong and T. Hornik, *Control of Power Inverters in Renewable Energy and Smart Grid Integration*, 1st ed. Chichester, West Sussex, United Kingdom: John Wiley and Sons, 2013.

[25] Visual Crossing Corporation. Weather Query Builder. [Online]. Available: https://www.visualcrossing.com/weather/weather-data-services. Accessed Aug. 26, 2022.

[26] Fluke Corporation, *Fluke 434/435 Three Phase Power Quality Analyzer User’s Manual*, 2008 [Online]. Available: https://dam-assets.fluke.com/s3fs-public/434_435_umeng0300.pdf

[27] Edvard, “Harmonic Distortion,” Electrical Engineering Portal, Nov. 23, 2010 [Online]. Available: https://electrical-engineering-portal.com/harmonic-distortion

THIS PAGE INTENTIONALLY LEFT BLANK

Initial Distribution List

1. Defense Technical Information Center
   Ft. Belvoir, Virginia

2. Dudley Knox Library
   Naval Postgraduate School
   Monterey, California